ROLE OF WAVE FORCING, STORMS AND NAO IN OUTER BAR DYNAMICS ON A HIGH-ENERGY, MACRO-TIDAL BEACH

Geomorphology

10.1016/j.geomorph.2014.07.025

Gerd Masselink[1], Martin Austin, Tim Scott, Tim Poate and Paul Russell

[1]g.masselink@plymouth.ac.uk

ABSTRACT

Outer sand bar dynamics on a high-energy macro-tidal beach were investigated using long-term (multi-year) field datasets of intertidal morphology and offshore bathymetry. Utilising a 15-year time-series of Argus video images, five distinct outer bar types were identified: Mega Rip, Longshore, Crescentic, Crescentic Attached and Welded. The most common classification was Crescentic Attached, with the outer bar oscillations being out of phase with the inner bar oscillations, as would be expected for the shore-normal wave approach at this site. The outer bar had a typical amplitude of 0.5–1 m and a longshore wavelength of 600 m. Changes in outer bar morphology were related to measured and modelled nearshore wave data. However, the outer bar morphology changed over a much longer time scale (monthly-to-annual) than the daily-to-weekly variations in wave height and period. An extended duration of energetic wave action was required to bring about an upstate bar transition to the Longshore or Mega Rip state, where the bar then remained arrested for a significant amount of time, requiring several months of low wave conditions to induce a down state transition through Crescentic to Welded. This slow morphological response is explained by extended relaxation times attributed to the large tidal range at the study site where the outer bar morphology is only active for part of the tidal cycle (several hours around low tide). The configuration and position of the outer bar were related: the more upstate (downstate) bar types being associated with a more offshore (onshore) bar position. The detrended outer bar position was significantly related to a forcing term based on wave power and disequilibrium of the dimensionless fall velocity with offshore (onshore) bar migration occurring when wave conditions were more (less) energetic that the antecedent conditions. The upstate end member (Longshore or Mega Rip) was attained sometime during the winter months for 14 out of the 16 years of monitoring; the outer bar remained attached to the low tide shoreline over the winter 2005/2006 and 2010/2011. These two winters with incomplete upstate cycles were characterised by the lowest winter wave conditions and negative winter North Atlantic Oscillation (NAO) indices, suggesting that the winter NAO is correlated with both beach state and nearshore bar configuration.

KEYWORDS

Beaches; beach state; beach classification; nearshore bars; storminess; NAO

HIGHLIGHTS

- We examine outer bar dynamics on a high energy, macrotidal beach
- Outer bar dynamics are governed by seasonally varying wave conditions
- Outer bar states: Longshore, Mega Rip, Crescentic, Crescentic Attached and Welded
- Beach state is related to the Northern Atlantic Oscillation (NAO) index

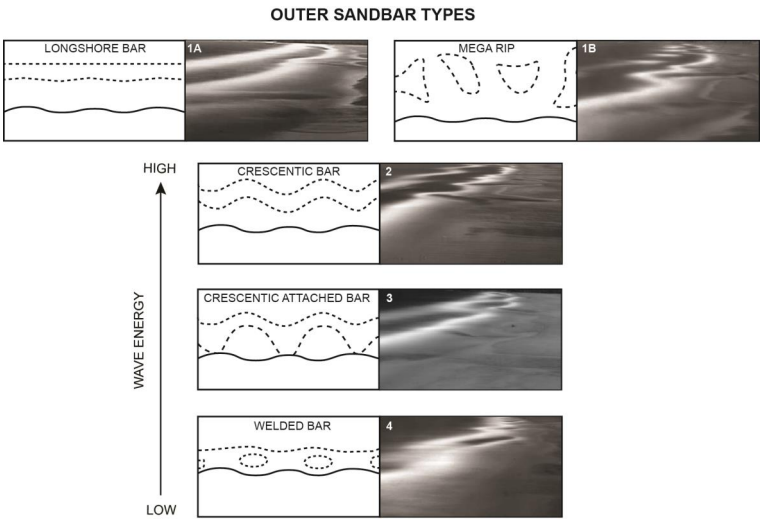

1. INTRODUCTION

The beach model proposed by Wright and Short (1984) considers wave-dominated beaches to be arranged across a spectrum of beach types, from reflective (steep), to intermediate (barred) and then dissipative (gentle-gradient) morphotypes, controlled by wave and sediment conditions. The different beach types can be predicted using the dimensionless fall velocity $\Omega = H_b/Tw_s$, where H_b is significant breaker height, T is peak wave period and w_s is median sediment fall velocity (Gourlay, 1968; Dean, 1973). Temporal changes in environmental conditions, quantified by Ω, drive concurrent changes in beach state, albeit with a lag due to relaxation time effects (Wright et al., 1985; Aagaard, 1988; Davidson et al., 2013).

This beach state model stimulated a large volume of subsequent research into the key factors controlling beach morphology. Some of these investigations sought to confirm the validity of the model by rigorously analysing more objective and extensive data sets (Lippmann and Holman, 1990; Ranasinghe et al., 2004). Other follow-up studies presented alternative models more suitable for different types of environments; for example, multi-bar beaches (Short and Aagaard, 1993; Short, 1992), low-wave energy settings (Hegge et al., 1996; Jackson et al., 2002) and large tidal environments (Short, 1991; Masselink and Short, 1993; Masselink and Hegge, 1995). More recently, studies along rocky coasts and embayed beaches highlighted the role of geology in constraining beach morphological development (Jackson et al., 2005), invoking the identification of distinctly different beach state models for geologically-controlled beaches (Loureiro et al., 2012). Nevertheless, the most comprehensive and rigorous longitudinal study of beach types so far by Scott et al. (2011), including almost one hundred wave-dominated, tide-affected and geologically-controlled beach settings in the UK, confirmed the general validity of the Wright and Short (1984) model.

Investigations into nearshore bar dynamics were carried out concurrently with and complementary to the beach state studies. Initially based solely on bathymetric surveys (e.g., Ruessink and Kroon, 1994), but more recently relying for its data collection on Argus video cameras (e.g., van Enckevort et al., 2004; Armaroli and Ciavola, 2011), these studies focus on the quantification and explanation of bar migration and evolution. Without exception, all research into outer bar dynamics has been carried out in either micro- or meso-tidal environments, i.e., settings with the mean spring tide (MSR) range less than 4 m. Intertidal bars are well known to occur in macro-tidal settings (e.g., Masselink and Anthony, 2001; van Houwelingen et al., 2006a, b; Sedrati and Anthony, 2007), but outer bars have only been reported from macro-tidal settings in passing (e.g., Austin et al., 2010, 2013, 2014; Scott et al., 2011;) and no systematic description of their morphology and dynamics has yet been presented.

In micro- and meso-tidal, wave-dominated settings, double (or even triple) outer bars are not uncommon. Invariably, the inner bar system is more three-dimensional than the outer bar system; the former tends to be of the welded and transverse bar type, whereas crescentic and linear bar configurations are more common for the latter (e.g., Price and Ruessink, 2011). Upstate (3D to 2D; offshore migration) and downstate (2D to 3D; onshore migration) transitions occur under increasing and decreasing wave energy conditions, respectively (Short, 1979; Lippmann and Holman, 1990; Ranasinghe et al., 2004; Poate et al., 2014), although longshore currents are also thought to play a role in straightening bar morphology (Price and Ruessink, 2011). There is also morphodynamic feedback between the outer and inner bar system; specifically, the outer bar protects the inner bar from energetic wave actions (Coco et al., 2014), whilst also controlling wave breaker patterns and nearshore current circulation over the inner bar system, even under less energetic wave conditions (Castelle et al., 2010a, b). According to Price and Ruessink (2011), the outer and inner bar systems are out-of-phase (in-phase) for dominantly parallel wave approach and weak longshore currents (oblique wave approach and strong longshore currents). Along many multi-barred coastlines, long-term (decadal) bar cycles have been identified, either characterised by offshore (Walstra et al., 2012) or onshore (Aagaard et al., 2007) bar migration.

In macrotidal environments, the large tidal range, and the associated pronounced tidal non-stationarity, is thought to inhibit the development of nearshore bar systems (Masselink, 1993). The tidal migration of the different morphodynamic zones (swash, surf and shoaling) are also expected to enhance smooth featureless beach profiles, more akin to the shoaling wave zone fronting microtidal beaches (Wright et al., 1982; Jago and Hardisty, 1984). Bar morphology is predicted to occur in macrotidal environments around low tide level and only if the relative tide range RTR, the ratio between MSR and the modal significant breaker height H_s is less than 7 (Masselink and Short, 1993). The beach described in this paper, Perranporth in the southwest of England, experiences a modal summer and winter wave height H_s of 1.1 m and 1.6 m, respectively, and a MSR of 6.1 m. Given a RTR value for this beach of 3.8–5.5 (and a modal Ω value of c. 5), bar morphology can be expected around the low tide level. However, in addition to an inner bar system just below spring low tide level, an additional outer bar is located in c. 3 m water depth at spring low tide. It will be demonstrated and argued that, despite the large absolute and relative tidal range, the studied beach at

low tide very much looks and behaves like a 'normal' micro- or meso-tidal double-barred beach (e.g., Gold Coast, Australia, Price and Ruessink, 2011; and Aquitaine coast, France, Senechal et al., 2009).

A description of the study area will be presented first (Section 2), followed by a comprehensive analysis of the wind regime, storm surge characteristics and the wave climate in the region, including the relation between winter storms and the North Atlantic Oscillation Index (NAO). The methods used to collect and analyse the morphological data set will be discussed in Section 3. The long-term outer bar dynamics derived from the 16-year Argus data set and the beach morphological response data based on the 2-year intertidal and subtidal beach surveys will be discussed next (Section 5). Finally, the morphological observations are then linked to the hydrodynamic forcing in the final results section (Section 6).

2. DESCRIPTION OF STUDY AREA

Perranporth beach in the southwest of England is typical of the open-coast beaches found along the 160-km length of the northern coast of the peninsula (Figure 1). This southwest region is a renowned tourist location with 5 million visitors annually and Perranporth is a notable tourist hotspot and surf beach. The 3.5-km long beach faces west-north-west towards the Atlantic Ocean and is backed by a combination of Devonian hard rock cliffs and coastal sand dunes. The beach is composed of medium quartz sand with a median grain size D_{50} of 0.28–0.34 mm and a sediment fall velocity w_s of 0.04 m s^{-1}. The beachface and intertidal zones are relatively flat, with an average gradient of 0.015–0.025, and the subtidal gradient up to 20 m water depth is c. 0.02. Perranporth is a high energy beach exposed to both Atlantic swells and local wind waves produced by the prevailing south-westerly winds. The average annual significant wave height H_s is 1.4 m, with an annual H_{max} of 5–8 m, based on analysis of the inshore directional wave rider buoy (DWR; see Figure 1). Wave approach is typically shore-normal. The tidal regime is semi-diurnal and macro-tidal with a mean spring and neap range of 6.3 m and 2.7 m, respectively. The largest spring tides occur during the equinoxes in September and March when the tide range may reach up to 7.3 m. Such large tidal range can generate strong tidal currents, and peak speeds are 0.4 m s^{-1} and 0.2 m s^{-1} during springs and neaps, respectively. Flows are along-coast, towards the north-east during the flood phase of the tide and the south-west during the ebb.

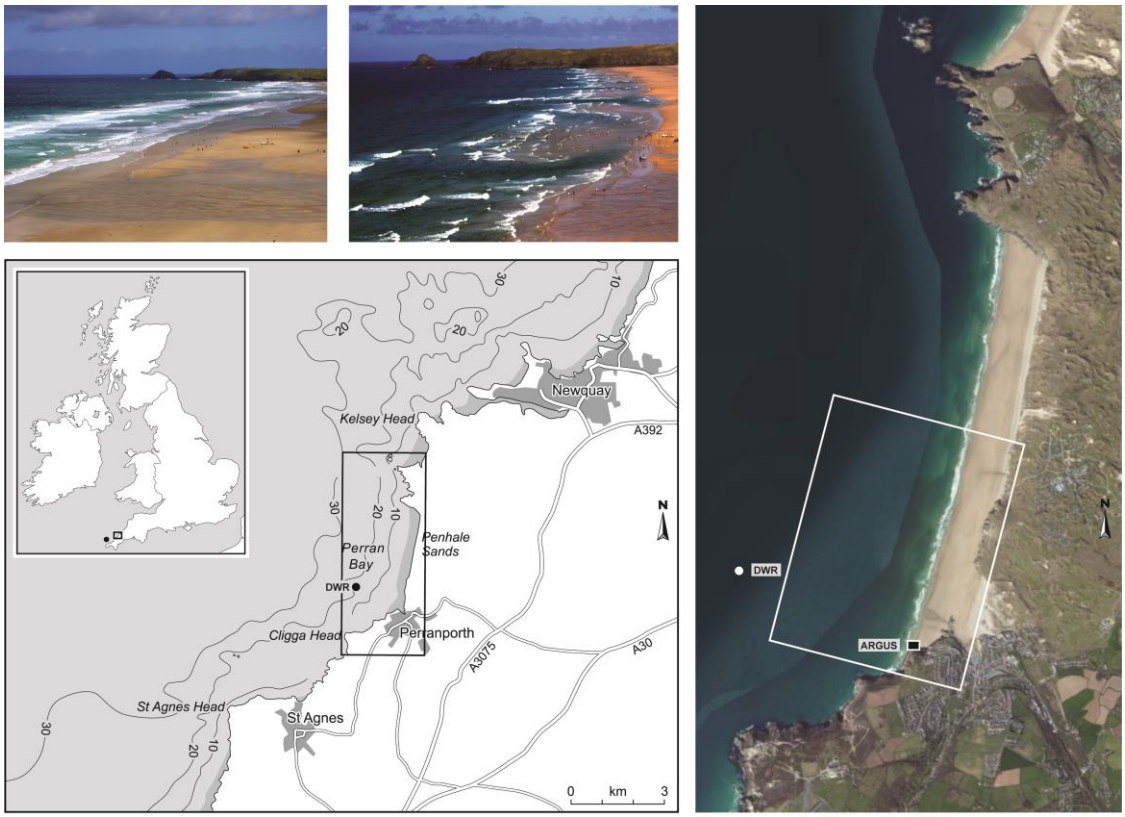

Figure 1 – *Description and location of the study area. The bottom-left panel shows location map and bathymetry of the region near Perranporth with the position of the directional wave rider buoy (DWR). The black rectangle on the map indicates the extent of the aerial photograph of the beach shown in the bottom-right panel, which also depicts the location of the DWR and the Argus video monitoring station (ARGUS) and the extent of the survey area (white rectangle). The two photos of Perranporth at the top of the figure, taken from the ARGUS position, illustrate the typical winter beach state (left) with a linear bar and the typical summer beach state (right) with pronounced transverse bar/rip morphology.*

Perranporth is classified as a low tide bar-rip beach according to the morphodynamic classifications of Masselink and Short (1993) and Scott et al. (2011), and further supported by long-term observations by Poate et al. (2014), with a 400–500 m wide intertidal zone, low-tide bar/rip morphology and a subtidal outer bar (Austin et al., 2013). Figure **2** shows the beach and nearshore morphology recorded at the end of winter in 2011. The morphology is typical of Perranporth and characterised by a relatively featureless intertidal zone, complex three-dimensional morphology around and just below the MLWS tide level and a crescentic-to-straight outer bar system (around x = 800 m). The typical crest elevation of the outer bar is -5 to -6 m ODN, which means that only under above-modal wave conditions and around low tide the outer bar experiences breaking waves. The inner bar system, on the other hand, experiences breaking waves every low tide, but only under energetic wave conditions during high tide.

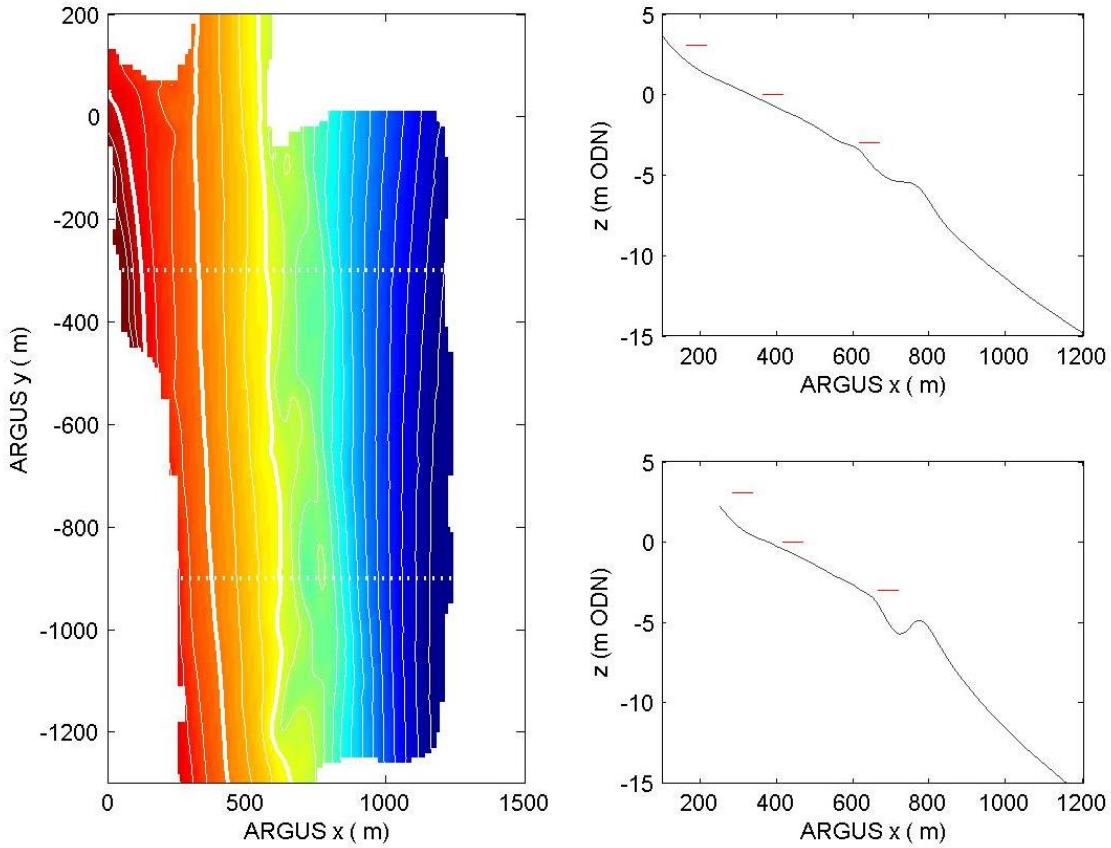

Figure **2** – *Left panel shows digital elevation model (DEM) surveyed on 28/04/11. Contour lines are at 1-m spacing, thick contour lines represent MHWS, MSL and MLWS, and horizontal dotted lines are the transects plotted in the right panels. The colour scale runs from -15 m ODN (dark blue) to 5 m ODN (dark red). Right panels show beach profile at* y = *-300 m (upper panel) and -900 m (lower panel), with short horizontal lines representing MHWS, MSL and MLWS.*

Perranporth has been the site of much previous coastal work. For example, some of the first observations of surf beat were made by Tucker (1950) at this site. In 1996 Perranporth was chosen as the site for the UK's first ARGUS video station (Davidson et al., 1997; Holman and Stanley, 2007) and these cameras remain operational to the present day. A series of swash experiments using arrays of in-situ instrumentation have been carried out on the high tide beach (Butt and Russell, 1999; Butt et al., 2001, 2002, 2005, 2007; Butt and Russell, 2005; Masselink et al., 2005; Masselink and Russell, 2006; Lanckriet et al., 2014; Puleo et al., 2014a, b). Since 2010, the site has also become a focus for studies on rip currents (Austin et al., 2010, 2013, 2014; Scott et al., 2014), their links to bather safety (Austin et al., 2013) and their influence on bedform dynamics (Thorpe et al., 2013). Intertidal beach changes on Perranporth, and comparison with other beaches in the region has been reported by Poate et al. (2014). Because Perranporth has been, and still is, a major field site for coastal scientists from Plymouth University, a large amount of data are available. An overview of these data are shown in Figure **3** and it is this data set which forms the basis of the analysis presented in this paper.

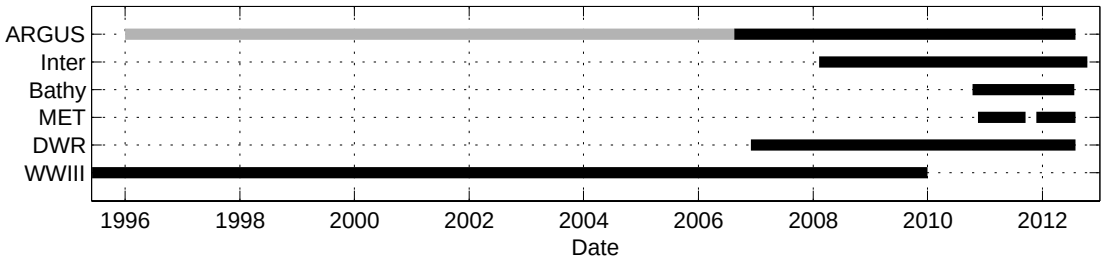

Figure **3** – *Timeline of the data sources available for analysis. From top: ARGUS video data (ARGUS), intertidal beach morphology (Inter), sub-tidal bathymetry (Bathy), meteorological data (MET), directional wave rider buoy (DWR) and Wave Watch III model output (WWIII). Grey bar represents early ARGUS data that has not been merged and rectified. The WWIII was provided by Guillaume Dodet and goes back to 1953.*

3. WIND, WATER LEVEL AND WAVE FORCING

3.1 Meteorological forcing

Meteorological data were recorded using a weather station installed at the same location as the Argus station on the headland at the southern end of Perranporth. The weather station consisted of an ultrasonic anemometer plus pressure and temperature sensors. This sensor was installed in Nov 2010, which is just over 2 months after the commencement of the subtidal bathymetric surveys (see Section **5**); there is also a 2-month period of missing data in autumn 2011. Data were sampled at 10-min intervals and logged together with the Perranporth directional wave rider buoy (DWR) maintained by the Channel coastal Observatory (see section **4.2**). Wind speed and direction data were smoothed with the application of a 5-point moving average filter. The 2-year time series of wind data and their statistical analysis plotted in Figure **4** shows a mean wind speed of 6.5 m s^{-1} and a maximum-recorded speed of 33 m s^{-1} on 15/12/10. Wind direction is highly variable, but the wind rose shows a dominance of winds from the west-southwest with northerly and easterly winds being of secondary importance. The highest wind speeds are associated with the south-westerly conditions.

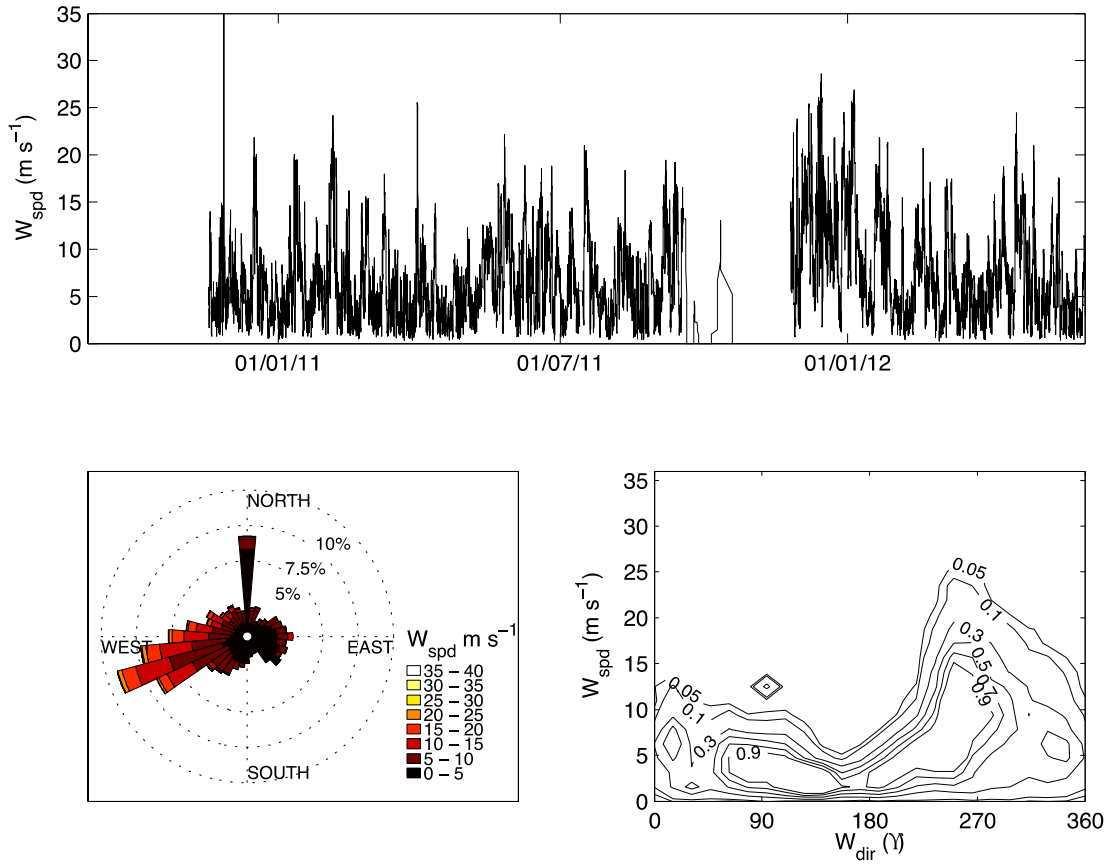

Figure **4** – *Analysis of 2 years of wind data collected at Perranporth. Top panel shows the time series of wind speed* W_{spd}. *Bottom left panel shows the wind rose and the bottom right panel shows the joint frequency distribution of wind direction* W_{dir} *and wind speed* W_{spd}.

3.2 Storm surge

Water level data were obtained from the UK Tide Gauge Network stations at Newlyn and Ilfracombe, located c. 75 km south and c. 110 km north of Perranporth, respectively. Data were sampled at 15-min intervals using bubbler-type gauges and are reduced to Admiralty Chart Datumn (ACD). Perranporth sits approximately 1/3 of the distance along the coast connecting Newlyn and Ilfracombe, so the tidal elevation η was computed from the data at these stations using a simple linear interpolation:

$$\eta_{PPT} = \eta_{NEW} + (\eta_{ILF} - \eta_{NEW}) \left[\frac{x_{PPT} - x_{NEW}}{x_{ILF} - x_{NEW}} \right] \quad (1)$$

where x is the along-coast coordinate of the stations and the subscripts PPT, NEW and ILF refer to Perranporth, Newlyn and Ilfracombe, respectively. A similar interpolation was used to compute the tidal residual Δz at Perranporth. Tidal elevations were subsequently converted to Ordnance Datum Newlyn (ODN), which is c. 0.2 m above mean sea level (MSL). Tidal stream data were extracted from the Admiralty Tidal Stream Atlas for each hour of the flood and ebb tide during springs and neaps at tidal diamond number SN055B. This is located at 50°21.93'N, 5°14.06'W, approximately 5.5 km offshore of Perranporth.

The 2-year time series of atmospheric pressure and water-level data is plotted in Figure 5. The barometric pressure provides an indication of the passage of deep Atlantic cyclonic depressions with associated weather fronts and the capacity to induce storm surges. A number of events with pressures falling below 990 mb occurred, with a lowest recorded barometric pressure of 969 mb during April 2012. Despite the frequent occurrence of relatively low pressure, the tidal residual indicates that the surge level at Perranporth is small and rarely exceeds 0.5 m. A number of the recorded positive surge events are clearly linked to periods of low barometric pressure, e.g., during February in 2011. Negative surges also occur and are related to high barometric pressure, e.g., during March in 2012.

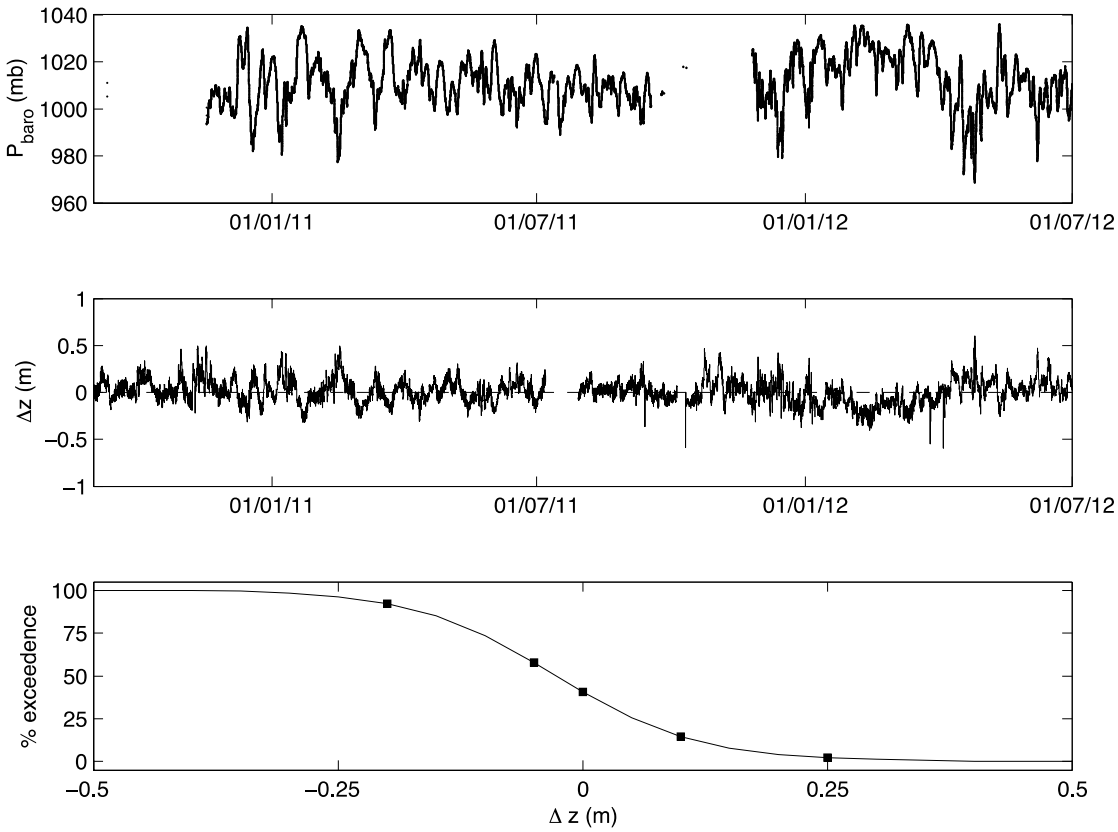

Figure 5 – *Upper two panels show 2-year time series of barometric pressure* P_{baro} *and residual water level* Δz *(measured water level minus predicted tide level). Lower panel shows percentage exceedance of residual water level, where the black squares indicate the 5, 25, 50, 75 and 95% exceedance levels.*

3.3 Wave climate

Data were collected by a Datawell Waverider III buoy moored in ~12 m of water depth at low tide directly offshore of the study site (see DWR in Figure **1**). Vertical heave, and north and west displacements were split into bursts, measured every 30 min, for 30 min at a rate of 1.28 Hz (n = 2304 data points). To characterise the wave climate, four integrated spectral parameters were computed from the directional wave spectra: (1) mean wave height; (2) spectral mean wave period; (3) spectral peak wave period; and (4) peak wave direction. The significant wave height H_s was calculated as:

$$H_s = 4\sqrt{m_0} \tag{2}$$

where m_0 is the zeroth moment of spectral density (total variance) given by:

$$m_n = \int_{f_f}^{f_c} f^n S(f) df \text{ with } n = 0 \tag{3}$$

where $S(f)$ is the spectral density at frequency f. The limits of the integration are the fundamental frequency f_f and the Nyquist frequency f_c, which correspond to 0.005 and 0.64 Hz for the Datawell buoy, respectively. The spectral mean period T_m was computed as:

$$T_m = \frac{m_0}{m_1} \tag{4}$$

where m_1 is the first moment of the spectral density, calculated as in Eq. (3) with n = 1. The spectral peak period T_p was computed as the period of the maximum spectral peak. The energy variance-density spectra $S(f)$ were computed from the vertical heave data using Welch's segment-averaging method with 9 segments with 50% overlap, giving ν = 18 degrees of freedom and a frequency resolution of 0.005 Hz. The normalised directional distributions $D(f,\theta)$ were computed from the heave and displacement data using the Maximum Entropy Method (MEM) following Lygre and Krogstad (1986).

The time series and analysis of the wave data shown in Figure **6** reveals highly variable wave conditions almost exclusively incident from the West with H_s = 0.5–8 m, T_m = 4–15 s and T_p = 6–22 s. The 50, 90 and 99% exceedence H_s and T_m are 1.14, 2.40 and 3.86 m, and 6.4, 8.8 and 11.0 s, respectively (not shown). There is, however, clear evidence of seasonality with typical summer and winter H_s of 1 and 1.5 m, respectively. The joint distribution of H_s and T_m further indicates that the larger waves tend to have the longer periods, and that the most frequently occurring wave condition is characterised by H_s = 1.1 m and T_m = 5.5 s. Spectral analysis of the wave data (not shown) further indicates that the majority of the wave energy is in the swell-wave region at frequencies of 0.07–0.12 Hz, but periods of high waves are characterised by a broader energy-variance distribution with frequencies of 0.05–0.2 Hz, indicating a mixture of swell and sea conditions.

The frequency analysis of the wave height distribution was used to determine the threshold for storm events (Figure **6** – upper panel). A storm event was defined as an event where the significant wave height H_s exceeded the 0.95 quantile (2.89 m). The initiation of a storm was defined as the time when the hourly-averaged H_s exceeded the 0.75 quantile (1.73 m); the end of the storm was the time when the hourly-averaged H_s returned below 1.73 m. Using these criteria, 107 storm events were identified over the 2006–2012 survey period. The majority of the storms occurred in the autumn-winter-spring (Oct–Apr) period, but particularly in 2007, 2009 and 2011, there were also stormy periods in the peak summer months (May–Jul). The mean peak storm wave height was 3.8 m (s.d. = 0.8 m) with the mean wave height throughout the storms duration of 2.5 m (s.d. = 0.3 m). Peak and mean storm wave periods were 12 s (s.d. = 3.1 s) and 8.3 s (s.d. = 1.5 s), respectively, and the mean storm duration was 66 h (s.d. = 49 h). Only 4 storms had a peak H_s exceeding 5 m (in 2007, 2008 and 2011), and the summers of 2008 and 2010 were characterised by extended periods without any storm events.

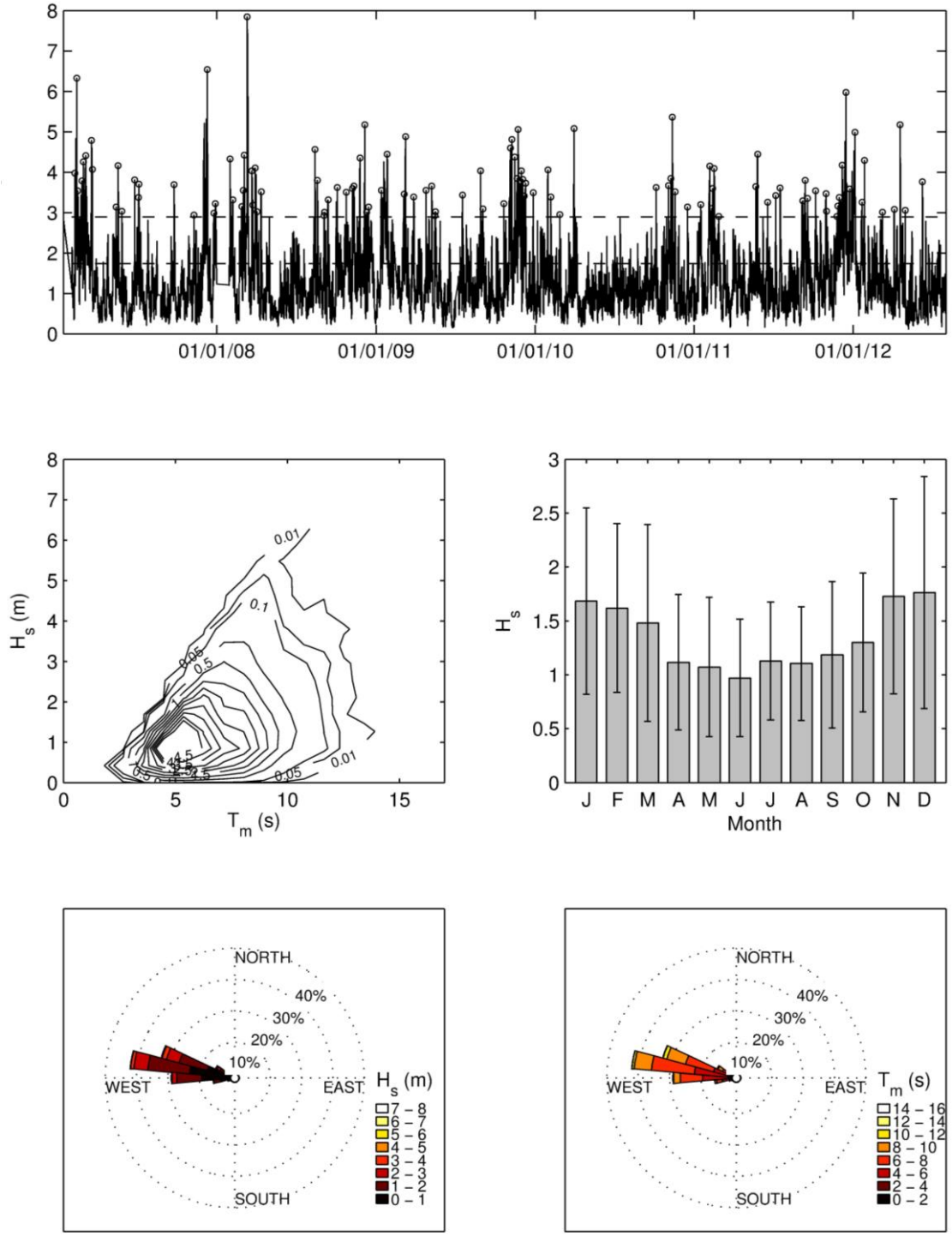

Figure **6** – *Wave climate for the 2006–2012 period computed from the Perranporth directional wave buoy. From top to bottom, and left to right: spectrally-derived wave height* H_{m0} *with identified storm events (defined as events where* H_s *exceeded 2.89 m); joint distribution of* H_s *and* T_m *with percentage occurrence contours; bar graph of the mean monthly* H_s *with error bars plotting 1 standard deviation of the mean; directional roses indicating the distribution of* H_s *and* T_m.

3.4 Link between winter NAO and wave climate

A 53-year combined record of modelled offshore wave data and winter North Atlantic Oscillation (NAO) index has been used to provide a longer-term context for the observations of outer bar morphodynamics discussed in this paper. The NAO is one of the major modes of atmospheric variability in the Northern Hemisphere and is particularly important in winter, when it exerts a strong control on the climate of the Northern Hemisphere (cf. Hurrell, 1996). The winter period between December and March exhibits the strongest inter-decadal variability and is strongly related to storm track (Osborne, 2006). Positive NAO index values are typically associated with stronger westerly dominated

winds across the northeast Atlantic (Dodet et al., 2010). It can be suggested that, through its control on the wind and wave conditions, NAO may affect inter-annual beach behaviour; however, evidence to date has been unconvincing (e.g., Thomas et al., 2012).

The extended winter NAO data for the period 1954 to 2012 used here were taken from the Climatic Research Unit, University of East Anglia web site (www.cru.uea.ac.uk). This NAO index follows Jones et al. (1997) and is the difference between the normalised pressures at Gibraltar and Reykjavik (southwest Iceland), and a positive NAO index means that the pressure differential is larger than normal (e.g., deep low pressure cells around Iceland). The associated wave forcing over this period was obtained from a 57-year hindcast (1953–2009) of the North East Atlantic wave climate with version 3.14 of the third-generation spectral wave model WAVEWATCH III (WWIII; Tolman, 2009), forced with re-analysed wind fields (Dodet et al., 2010). Figure 7 shows the 4-month winter-averaged (December-March) time series of hindcast wave heights for offshore location 50.10˚N 60.10˚W, 70 km to the southwest of Perranporth (water depth > 50 m). Significant correlations (r = 0.64 and 0.51) between winter NAO regional atmospheric forcing and winter-averaged H_s and Ω were identified (Figure 7). These relationships are examined further by Dodet et al., (2010), highlighting the location-specific nature of relationships between wave climate variability (H_s, T_p and D_p) and WNAO. Their analysis suggested that higher correlations between winter NAO and wave heights existed at higher latitudes.

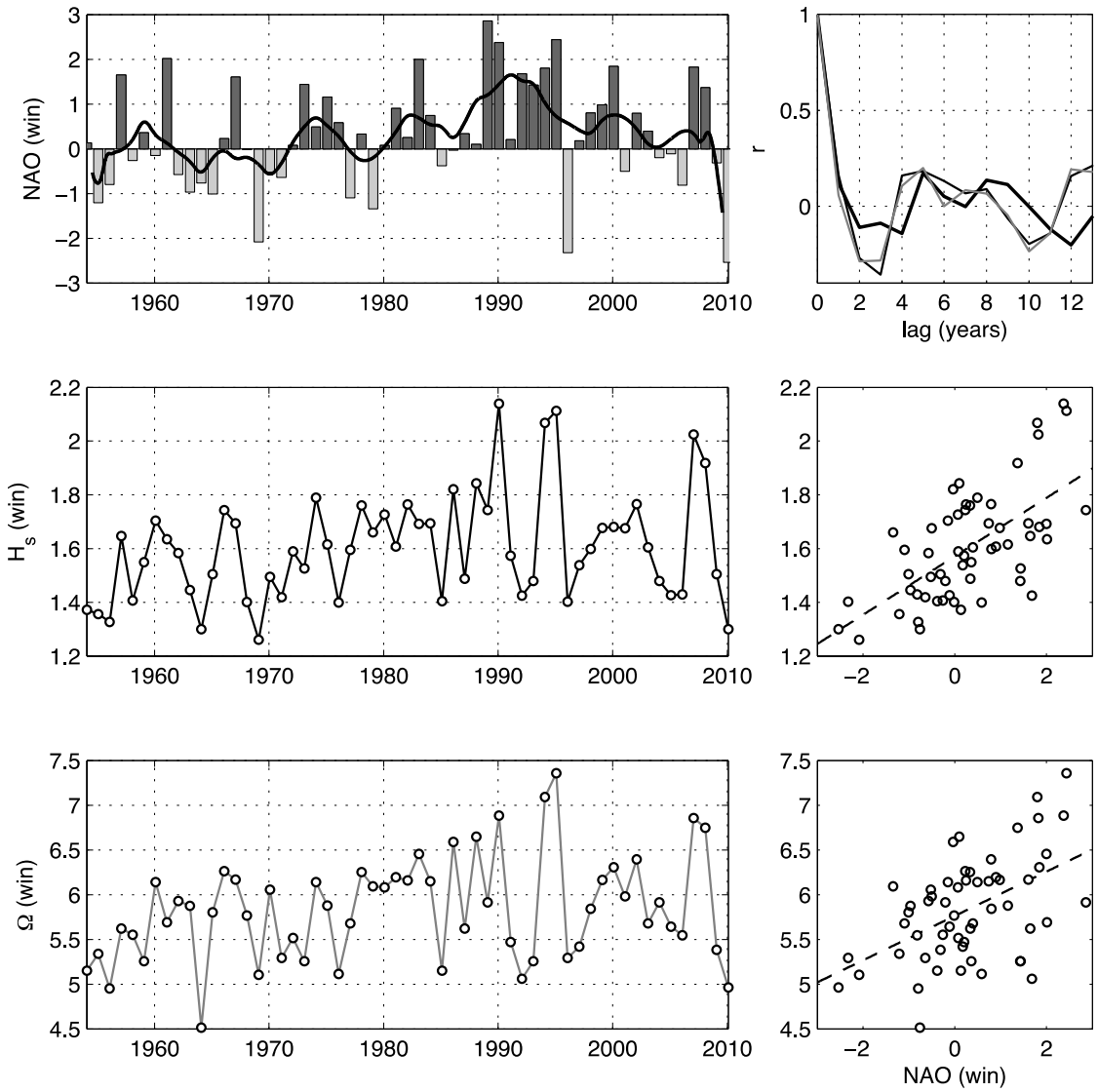

Figure 7 – *Long-term variability in winter NAO and hindcast wave climate obtained using the WWIII model. Upper left panel shows time series of winter NAO index (bars) with the 5-year low-pass filtered time series (bold line). Middle left panel shows time series of the winter-averaged offshore* H_s. *Lower left panel shows time series of winter-averaged values of he dimensionless fall velocity* Ω *using characteristic sediment fall velocity for Perranporth* (w_s = 0.04 m s^{-1}). *Upper right panel is autocorrelation function of winter NAO (bold black line),* H_s *(black line) and* Ω *(grey line). The middle and lower right panels show the relationship between winter NAO and* H_s *(middle) and* Ω *(lower), and the dashed line represents the least-squares best fit.*

Autocorrelation analysis of both wave H_s (winter) and winter NAO identified weak, but significant correlations (r = 0.2) at lags of 4–5 years (Figure 7 – upper-right panel) and this multi-annual cyclical behaviour is also evident in the 5-year low-pass filtered time series of winter NAO (Figure 7 – upper-left panel). It is clearly important to consider these identified longer-term inter-annual cycles in key forcing variables linked to beach change when interpreting the representativeness of short-term datasets of beach change.

To assess the representativeness of the WWIII dataset in describing forcing at Perranporth the hindcast offshore WWIII and measured nearshore Perranporth wave records for the period 2007–2009 were compared. Analysis showed that there was a strong (r^2 = 0.81) linear relationship between predicted and measured wave height (not shown): $H_{s,meas} = 0.61H_{s,\,mod}$ (RMSE of 1.01). The relationship becomes increasingly non-linear above 5 m, but as the 0.99 quantile is 3.86 m it was deemed appropriate to linearly adjust the offshore WWIII modelled H_s to represent the nearshore wave forcing.

4. COLLECTION AND ANALYSIS OF MORPHOLOGICAL DATA SET

Morphological data were collected using a combination of RTK-GPS mounted on ATV for the inter- and supratidal zone (cf., Poate et al., 2014), and echosounder with RTK-GPS mounted on jet-ski for the subtidal region. A total of 17 combined surveys of the supratidal, intertidal and subtidal zones were carried out from 15 October 2010 to 26 July 2012. Several surveys were carried out in quick succession during June and October 2011 associated with two intense field campaigns investigating rip currents on Perranporth beach (Austin et al., 2014; Scott et al., 2014), but most surveys were taken quasi-regularly every 2 months. Data from the two regions were combined into a 1.2 km x 1.2 km area and Loess-interpolated (Plant et al., 2002) to achieve 10-m grid resolution.

Considering the large width of the beach, the observed inner- and outer bar morphology is rather subtle and to gain better insight into the bar characteristics the residual morphology was computed. This was done by first taking a subsection of the DEM (x = 400 to 1000 m; y = -100 to -1200 m) that contains only the bar morphology (Figure 8 – left panel). Then, for each alongshore position at 10-m intervals a linear trend was least-squares-fitted to the cross-shore profile. This linear trend, which represents the planar gradient for that profile, was then subtracted from the profile to obtain the residual morphology, which clearly illustrate the inter- and outer bar morphology (Figure 8 – right panel). The linear trends fitted to the cross-shore profiles were remarkably constant with a mean value of 0.0185 and a standard deviation of 0.0003.

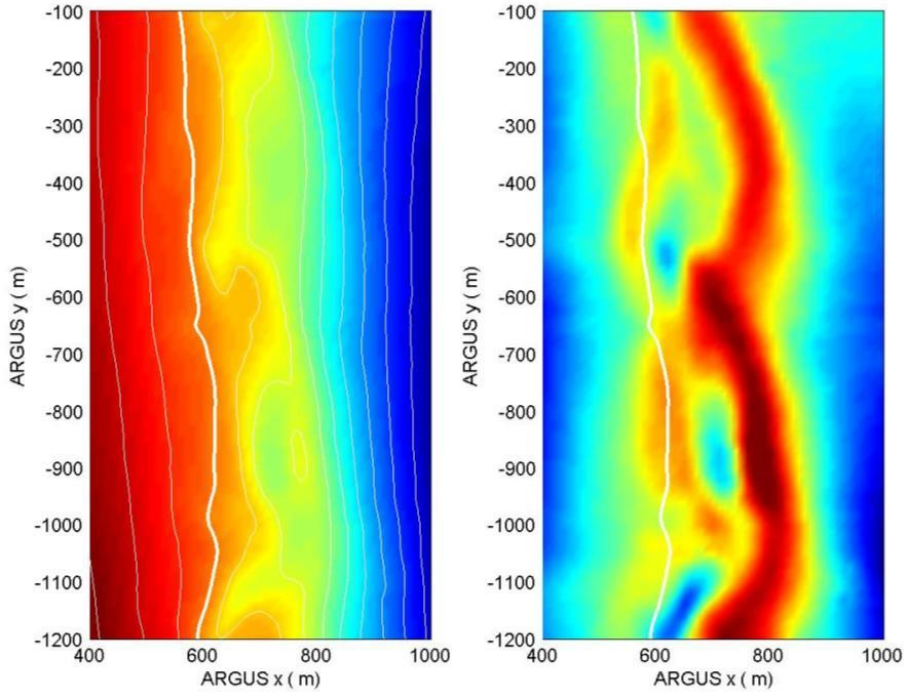

Figure 8 – *Left panel shows digital elevation model (DEM) of sub-section of beach with inner and outer bar morphology surveyed on 28/04/11. Contour lines are at 1-m spacing, the thick contour line represents MLWS, and the colour bar runs from -12 m ODN (dark blue) to 0 m ODN (dark red). Right panel shows residual morphology obtained by subtracting linear trend from each of the cross-shore profiles. The contour line represents MLWS and the colour bar runs from –1.3 m (dark blue) to 1.3 m (dark red).*

In addition to providing a better visual representation of the inter- and subtidal bars, the residual morphology was also used to extract quantitative measures of bar morphology. For each of the survey data sets, the residual morphology was alongshore-averaged and the mean position of the outer bar crest x_c was determined from the average residual profile. The position of the bar crest was cross-referenced with the alongshore-averaged morphology to extract the mean elevation of the bar crest z_c. The standard deviation of the alongshore-averaged residual morphology was used as a surrogate for bar amplitude A_z and separate values for A_z were computed for the inner bar system (x = 400–650 m) and the outer bar (x = 650–1000 m). Finally, for each survey the position of the outer bar crest was extracted from the residual morphology (not the alongshore-averaged residual profile) and the standard deviation of the outer bar crest line was used as a surrogate for the longshore variability in bar crest position A_x.

Visual assessments of the low tide beach morphology, specifically the outer bar state configuration, were made from daily low water time-exposure and variance video images from an Argus camera system deployed on a headland to the south of the beach (Droskyn Point; elevation c. 45 m). Images were selected from low water periods where sea surface elevations were between -3.5 and -2.2 m ODN and significant wave heights were greater than 0.5 m. The daily image time series extends from August 1996 until 2012, with images at 30-min intervals.

Rectified plan-view Argus images were generated for the period 2006–2012 in line with standard image processing techniques, based on local geometries and using in-situ measurements as outlined in Holland et al. (1997). No reliable geometries are available for the earlier Argus images (1996–2006). The detection of bar-line position, through rectified images, is based on the wave breaking position, driven by water depth and wave height, which provides a proxy signal for bar location. For highly dissipative and macro-tidal sites the rapid migration of the shoreline across the beachface reduces the period of wave breaking over the outer bar and this can subsequently reduce the accuracy of bar position (Kingston et al., 2000; van Enckevort and Ruessink, 2001). To improve accuracy of the bar position estimates, image selection was limited to periods when H_s was between 0.5 and 1.5 m and tidal elevation was between -3.5 and -2.5 m ODN.

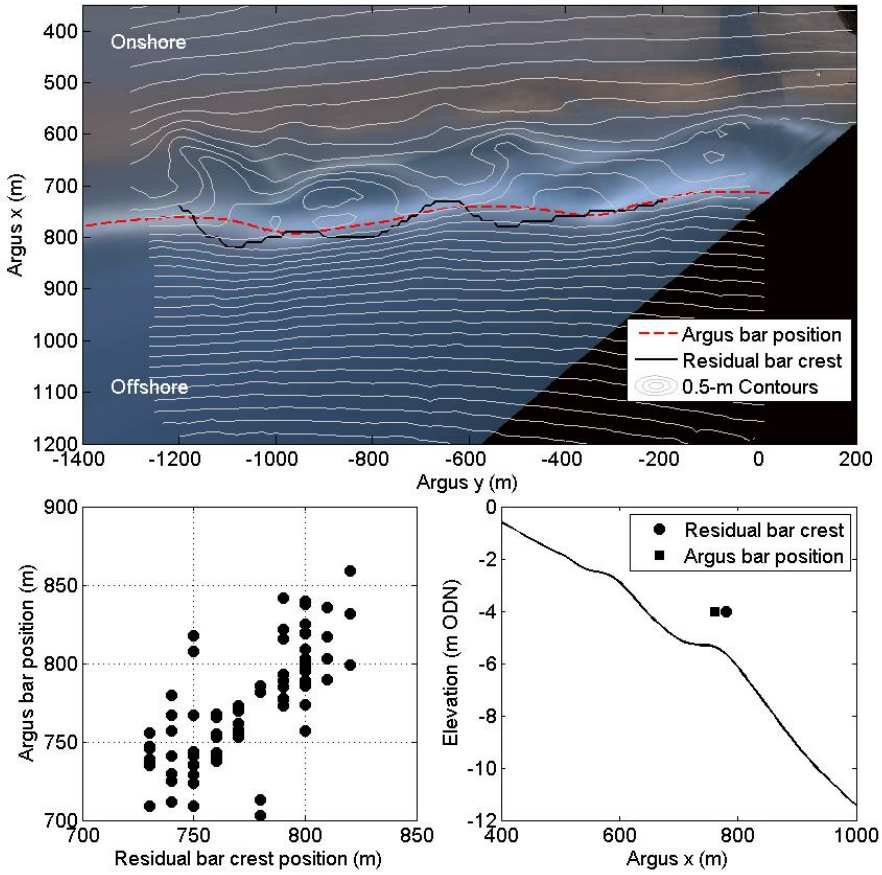

Figure **9** - *Rectified plan view Argus image from 20/04/11 with outer bar position (red dashed line), residual bar crest position (black solid line) and bathymetry contours at 0.5-m intervals (upper panel). Comparison between residual bar crest and Argus-derived bar position at various alongshore locations (bottom-left panel). Cross-shore profile (x = -500 m) showing the alongshore-averaged location of the bar position as defined by the residual morphology (circle) and the Argus image (square) (bottom-right panel).*

Prior to digitization of bar positions from rectified images, a validation of the technique was undertaken through comparison of bar location x_c derived from the bathymetric surveys with those identified using the semi-automatic BLIM toolbox (Figure **9** – upper panel). The alongshore variation in bar position between the techniques reflects the smoothing used in the BLIM approach, while the overall trend is well presented. Relative bar positions overlaid on the cross-shore profile further supports this approach (Figure **9** – lower panels).

5. OUTER BAR CLASSIFICATION AND BEACH MORPHOLOGICAL RESPONSE

5.1 Outer bar state classification and transitions

The 15-year time series of Argus video images was inspected to classify the outer bar morphology. The emphasis is on the outer bar state, because this bar is most pronounced (cf. Figure **8**); the inner bar is often difficult to distinguish from the shoreline (swash zone) and is generally not characterised by a distinct trough. Specific wave and tide conditions are required to be able to identify the outer bar in the timex and variance images and there were extended periods of time that no information on the outer bar configuration was available. For example, if wave conditions are too modest and/or tidal levels are too high, no breaking will occur on the outer bar to bring out its morphology, or indeed, confirm its presence. Nevertheless, 5 distinct outer sand bar types were identified (Figure **10**): Mega Rip (MR), Longshore (L), Crescentic (C), Crescentic Attached (CA) and Welded (W). On one occasion a triple bar state was observed (end of 2009). The outer bar types L, C, CA and W refer to the alongshore shape and position of the outer bar, whereas the MR type refers to deep and extensive rip channels dissecting the outer, and possibly the inner, bar morphology (Figure **10**). Therefore, the MR type does not refer to the large topographically-constrained rips channels as described by Short (1985). It should also be pointed out that although the L, C, CA and W outer bar types show similarity with the intermediate beach states of the Australian beach model (LBT, RBB, TBR and LTT; Wright and Short, 1984), the former specifically relate to the outer bar configuration of a modally double-barred beach, whereas the latter refer to the beach state of a single barred beach.

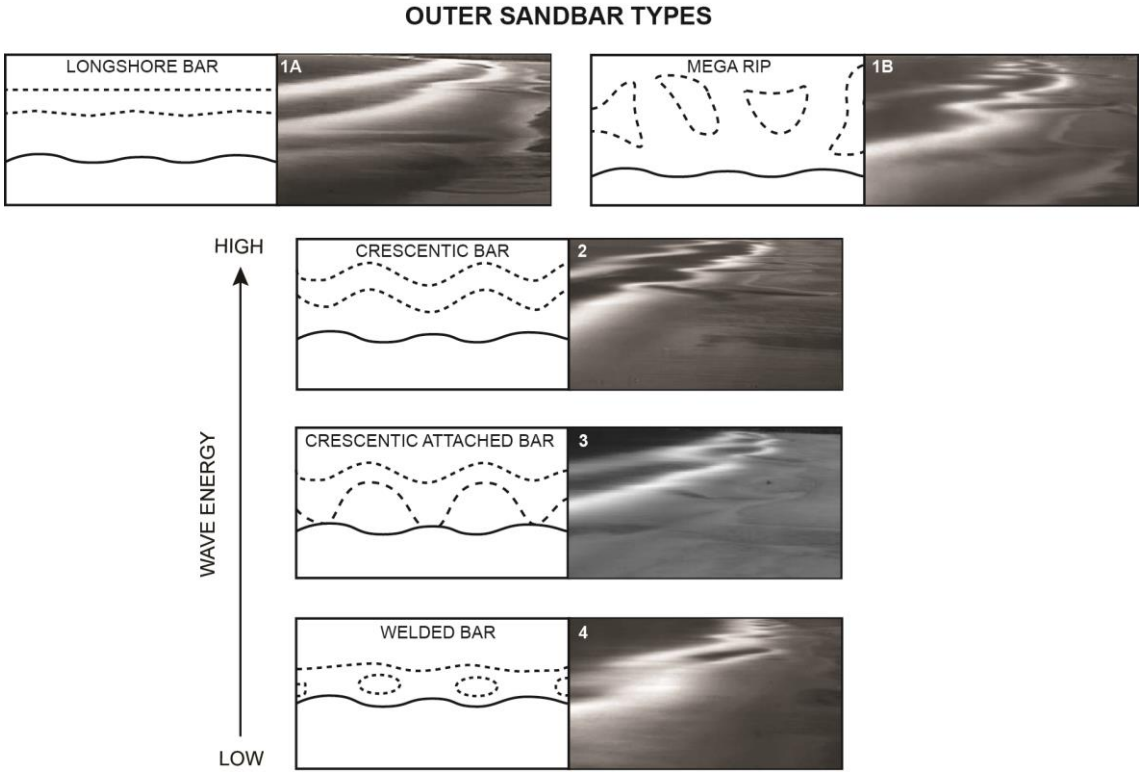

Figure **10** – *Schematic overview of defined outer bar states with example timex video images from Perranporth. Inner bar states are not defined.*

The frequency of occurrence of the different outer bar types and the wave conditions characterising their occurrence are indicated in Table **1**. The CA bar state was the most commonly observed and is associated with wave conditions closest to the mean long-term wave height ($<H_s>$ = 1.23 m). The least observed states were the W and L bar states which occurred at the low- and high-energy extremes in $<H_s>$ conditions, respectively. The C, MR and L bar states were associated with the highest values of $<H_s>$. Interestingly, L was the only bar state to have a modal offshore wave direction that deviated (-5°) from the long-term modal value. This may suggest that an increased angle from shore-normal encourages the development of a linear bar state that is dominated by longshore currents. MR bar states are

linked to the largest $<T_m>$ (Table 1). In some cases the outer bar merges with the inner bar and the beach becomes a single-barred beach.

Table 1 – *Statistics of observed outer bar states. The number of days with outer bar observations (959 days) is much smaller than the number of days over the 16-year period (5863). This is because there were a very large number of days with poor quality images or unsuitable wave/tidal conditions for making robust observations.* $<H_s>$ *and* $<T_m>$ *are the preceding 30-day means. Wave statistics were based on the offshore WWIII data adjusted to best represent the Perranporth inshore wave conditions measured at the DWR.*

Bar type (outer bar)	**Daily frequency (1996–2012)**	**Occurrence (n yr^{-1})**	**$<H_s>$ (m; adjusted)**	**$<T_m>$ (s; adjusted)**
Mega Rip (MR)	161 (16.8%)	10	1.53	6.8
Longshore (L)	50 (5.2%)	3	1.49	6.5
Crescentic (C)	208 (21.7%)	13	1.55	6.5
Crescentic Attached (CA)	420 (43.8%)	26	1.23	6.1
Welded (W)	120 (12.5%)	8	1.03	5.7
N bar obs.	959	-	-	-
All	5863	-	1.22	6.1
Bar resets (growth of outer bar; sig. transitions to L or MR states) occurred 14/16 winters				
Bar welds (welding of outer and inner bar; sig. transitions to W states) occurred 7/16 summers				

The time series of outer bar type shown in Figure **11** was inspected together with the complete timex time series (not shown) and indicates that the summer-winter seasonal variability in the wave climate (wave height) is the dominant control on the outer bar development. From the observation of outer bar type, a re-setting or partial re-setting of the outer bar, i.e., an upstate transition from W, CA or C to L or MR, occurred during 14 out of 16 winters (88%). The only winters where the outer bar was not observed to reach the most erosional state (MR or L) was during 2005/2006 and 2011/2012. Downstate transition from a detached outer bar type (C, L or MR) to a welded outer bar (W) was also observed. Such transition requires a prolonged lower energy summer period, often preceded by less energetic and shorter winters, and only occurred during 7 out of 16 summers (44%). A detailed analysis of the correlation between wave forcing and outer bar morphological response will be presented in Section **6**.

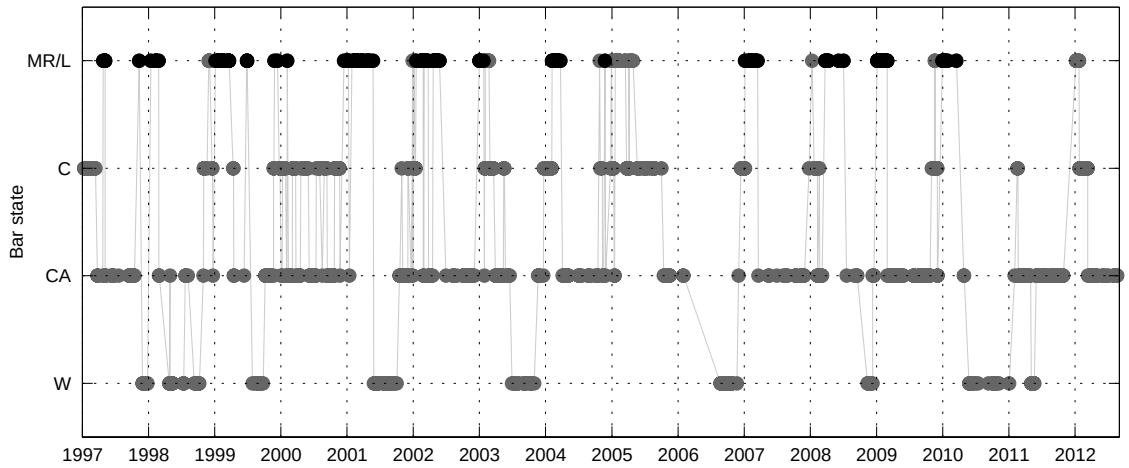

Figure **11** – *16-year time series of outer bar type. The 5 outer sand bar types are MR = Mega Rip (black circles); L = Longshore (grey circles); C = Crescentic; CA = Crescentic Attached; and W = Welded. Upstate and downstate transitions represent moving up and down the diagram, respectively.*

5.2 Beach and subtidal morphological change

The individual DEMs obtained over the 2-year survey period were used to quantify the maximum envelope of change dz_{max} by determining the difference between maximum and minimum profile elevations (i.e., the thickness of the

sweep zone or the envelope of change). By far the greatest profile variability, with dz_{max} in excess of 2 m, occurs in the subtidal zone (and around the MLWS level), from x = 600 to 1000 m, and is related to bar and rip channel dynamics, with dz_{max} values in the intertidal zone always less than 1 m and mostly less than 0.5 m (Figure **12** – left panel). The dynamic nature of the bar region compared to the intertidal area is also evident from the sweep zone of individual cross-shore profiles (Figure **12** – right panels), which suggests that morphological changes beyond -12 m ODN are within the error-bound of the subtidal measurements (c. 0.3 m).

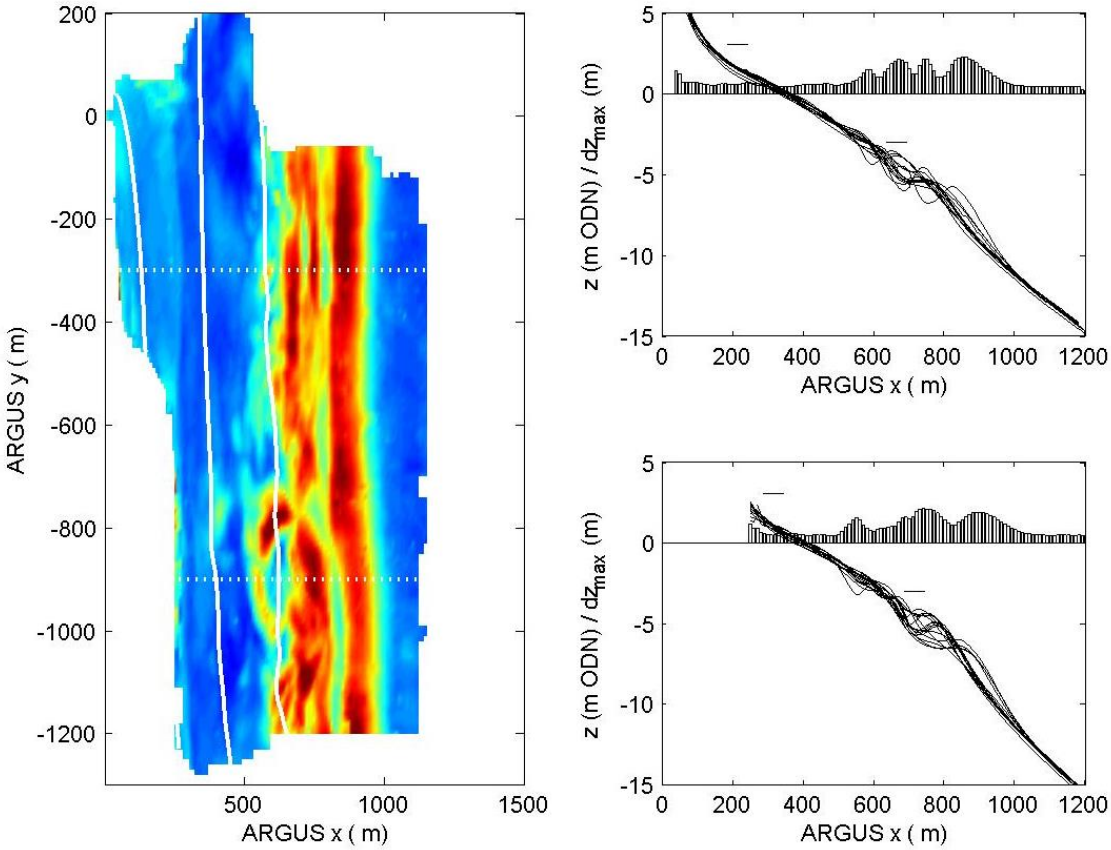

Figure **12** – *Left panel shows the maximum morphological change recorded over the survey period. The contour lines represent MHWS, MSL and MLWS, and the horizontal dotted lines represent the transects plotted in the right panels. The colour scale runs from 0 m (dark blue) to 2.2 m (dark red). Right panels show all 17 beach profiles at* y *= -300 m (upper panel) and -900 m (lower panel) and the maximum morphological change* dz_{max}. *The short horizontal lines represent MHWS and MLWS.*

The DEM of the residual morphology in the bar region was introduced in Section **4** (refer to Figure **8** – right panel) and clearly illustrates the characteristics of the inner- and outer bar morphology. The salient features are: (1) the amplitude of the outer bar system (c. 1 m) is significantly larger than that of the inner bar system (c. 0.5 m); (2) the outer bar is crescentic and is out-of-phase with the inner bar system (cf. Price and Ruessink, 2011); (3) the longshore wave length of the outer bar is c. 600 m; and (4) there is some indication that the inner bar system is nested with the large outer bar crescents and has a wave length of c. 300 m; however, the alongshore coverage of the survey is insufficient to confirm this latter suggestion. It is also noted that whereas the outer bar appears to have a distinct entity, the inner bar morphology is more disjointed (by rip channels) and is more appropriately referred to as a bar system.

Figure **13** shows all the DEMs of the residual beach morphology over the 2-year survey period, again focussing on the region with inner and outer bar morphology (x = 400 to 1000 m; y = -200 to -1150 m). The bar configuration varied considerably over time, both in terms of alongshore variability (e.g., linear bar systems on 30/11/10 and crescentic bar systems on 20/10/11) and prominence (e.g., very pronounced outer bar on 17/01/12 compared to other surveys). There is also a strong indication that the bar systems migrated towards the south (positive y-axis) over the survey period. By tracking inner/outer bar merges and/or distinct outer bar horns over the survey period, an alongshore migration rate of 1–2 m day can be derived (white circles = 600 m in 9 months; black circles = 500 m in 14.5 months; Figure **13**). The anti-phase relationship between the inner bar system and the outer bar alluded to previously is evident in most of the DEMs and is, not surprisingly, clearest when the three-dimensionality of the bar systems is most pronounced (i.e., during the middle part of the survey period). Cross-shore bar migration is difficult to perceive on the DEM, but it is noted that there does seem to be a relatively sudden offshore migration of the complete outer bar system from

20/10/11 to 17/01/12, accompanied by significant straightening of the outer bar, but increased three-dimensionality of the inner bar system. It is further noted that at the start of the survey period (15/10/10) only an inner bar system was present, but that by the time of the second survey (13/11/10), a pronounced and linear outer bar had developed.

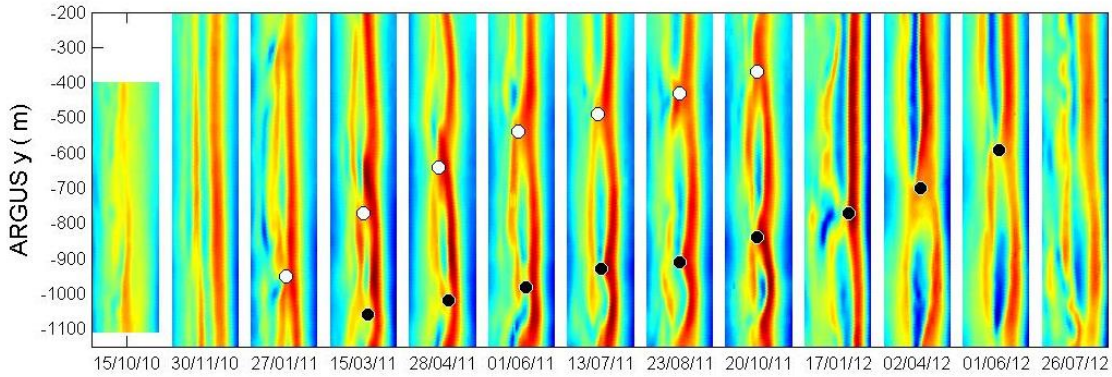

Figure **13** – *Residual morphology of sub-section of beach with inner and outer bar systems (*x = *400 to 1000 m;* y = *-200 to -1150 m). The colour bar runs from –1.3 m (dark blue) to 1.3 m (dark red). For each of the two intensive field campaigns only one survey is included, so the total number of surveys is 13. The white and black circles represent the position of inner/outer bar merges and/or distinct outer bar horns, and illustrate the southward migration of the outer bar morphology.*

The residual morphologies plotted in Figure **13** were used to extract the following quantitative measures of bar morphology: the mean position of the outer bar crest x_c; the mean elevation of the outer bar crest z_c; the bar amplitude A_z; for the inner bar system (x = 400 –650 m) and the outer bar (x = 650–1000 m); and the longshore variability in bar crest position A_x (refer to Section **4** for a definition of these parameters). Time series for these bar parameters are shown in Figure **14**. The time series of bar crest position x_c shows that the outer bar migrated c. 150 m offshore during the survey period with three occurrences of particularly large offshore migrations (> 50 m) and two occurrences of significant onshore migration (Figure **14** – upper panel). As the outer bar migrated offshore, the bar crest elevation z_c progressively reduced, by up to 1.5 m over the survey period, and the largest reductions in z_c coincided with the greatest offshore bar migrations (Figure **14** – second panel). Time series of the bar amplitude A_z demonstrates that the outer bar is c. twice as pronounced than the inner bar system, and also that the bar amplitude remained relatively constant throughout the survey period (Figure **14** – third panel). The only observation of note is that during the offshore outer bar migration event documented by the 17/01/12 survey the outer bar increased in prominence (A_z from 0.6 to 0.7 m), while the inner bar system became more subdued (A_z from 0.3 to 0.1 m). The longshore variability in bar crest position A_x increased over the course of the survey and indicates that the outer bar became increasingly crescentic (Figure **14**– fourth panel). Straightening of the outer bar (corresponding to reduced A_x) coincided with offshore bar migration.

Time series of bar characteristics were compared with the time series of cumulative change in beach sediment volume (Figure **14** – bottom panel). The change in sediment volume relative to the second beach and nearshore survey (the first survey only had limited coverage) was computed using the same part of the beach for each survey so the volumetric changes are directly comparable. To investigate cross-shore sediment exchange, the beach was subdivided into 3 regions: (1) the upper part of the beach x = 0–500 m; (2) the inner bar region x = 500–700 m; and (3) the outer bar region x = 700–1000 (cf. Figure **12**). The total beach volume was obtained by summing across the three regions, and thus represents x = 0–1000 m. The region seaward of the outer bar (x = 1000–1200 m) was not included in the analysis, because it was considered that the accuracy of the measurements is of the same order as the morphological change (c. 0.3 m). For each zone, the total change in beach volume in m^3 was obtained by summing the elevations across the region, multiplying by 100 (the DEMs are at a 10-m grid resolution; therefore each grid point represents a 100 m^2 area) and relating this to the sediment volume at the start of the survey period.

The total beach sediment volume shows a progressive increase over the 2-year monitoring period (Figure **14** – bottom panel). By the end of the survey period the beach had gained 150,000–200,000 m^3 of sediment and, considering a beach length of 1200 m, this represents a gain of more than 10 m^3 per unit m beach width. This is unlikely to reflect a long-term accretionary trend and is interpreted as a response to a major erosion event that occurred prior to the commencement of the survey programme. The vast majority of this sediment accumulated in the outer bar region; in fact, both the upper beach region and the inner bar zone showed no significant difference between the start and end of the survey period. Considering a surface area for the outer bar region of 360,000 m^2 (300 m x 1200 m), this implies an increase in the elevation of this region of 0.4–0.5 m. Perhaps, surprisingly, there is limited linkage between the upper

beach and the inner bar region, and the outer bar region. The substantive increase in outer bar sediment volume is sourced from outside the survey area, either from an offshore source or through longshore transport, and certainly not from the upper part of the profile. The only strong indication of a cross-shore sediment exchange is apparent for the period 28/10/11 to 17/01/11, when the outer bar migrated offshore by c. 100 m and large rip channels were scoured out in the inner bar zone. During this period, the outer bar region gained c. 150,000 m^3 of sediment, whereas, collectively, the upper beach and the inner bar region lost about the same amount. Clearly, during this period the erosion of the upper part of the beach fuelled the accretion in the outer bar region.

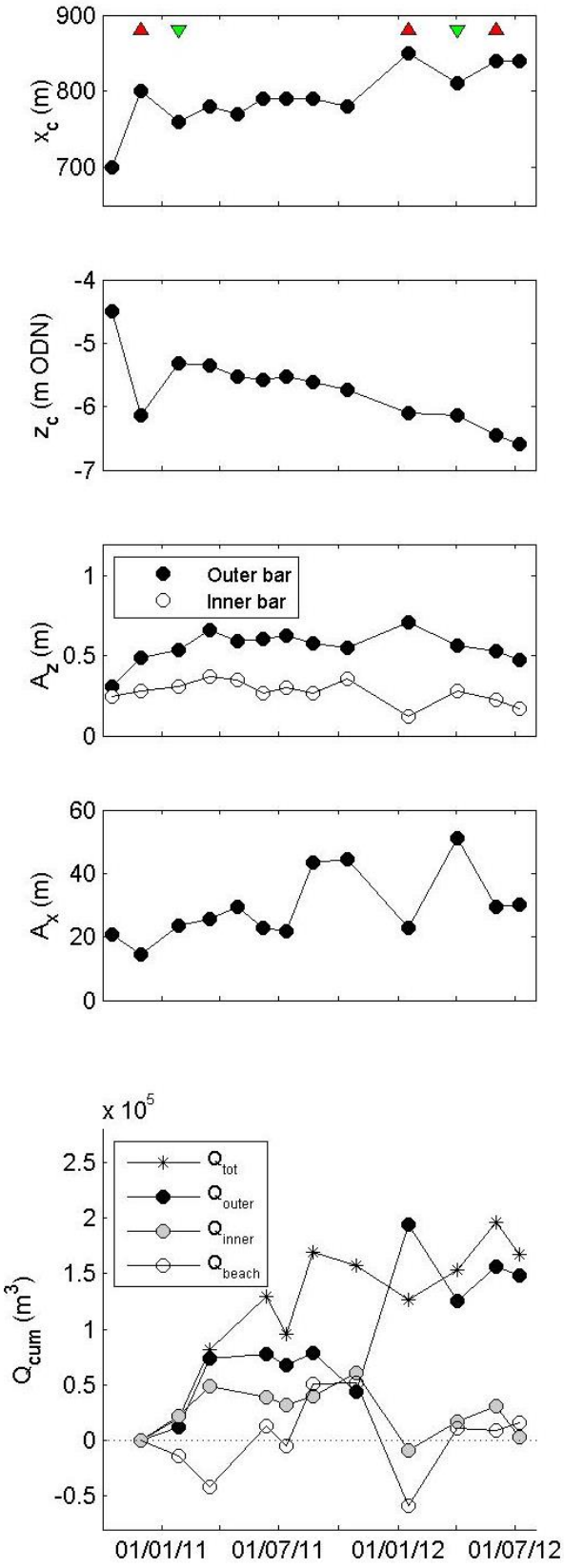

Figure **14** – *Upper panels show time series of quantitative measures of bar morphology: mean outer bar crest position* x_c*, mean outer bar crest elevation* z_c*, outer bar amplitude* A_z *and longshore variability in outer bar crest position* A_x*. The red (upward pointing) and green (downward pointing) triangles in the top panel indicate significant offshore and onshore outer bar migration, respectively. Lower panel shows time series of change in sediment volume for the upper beach, inner bar region and outer bar region. The total beach volume was obtained by summing across these three areas.*

The Argus data were used to extend the time series of the outer bar crest location over the period 2006–2013 and were compared with the outer bar state (Figure **15**). The position of the outer bar crest derived from the subtidal surveys collected over the period 2010–1012 are included in this figure. Despite the gaps in the time series of Argus-derived outer bar crest position, there is a clear link between onshore (offshore) bar migration and downstate (upstate) bar stage transitions. Two bar migration phases particularly stand out. The first phase was a 5-month period (Dec 2009 – Apr 2010) of sustained small waves (hence the lack of available images) and few storm events during which the outer bar migrated 50–100 m onshore. The second period relates to a distinct offshore-directed shift in bar position over a similar distance, which occurred over a 2.5-month period from the end of October 2011 to the start of January 2012. Wave conditions during this offshore bar migration included a number of energetic wave events. These bar migration phases relate closely to upstate and downstate shifts in the observed bar state. For the winters 2006/2007, 2007/2008 and 2009/2010 offshore bar migration also coincided with the development of Mega Rip outer bar state. While there is scatter in the dataset, which is largely attributed to differing hydrodynamic conditions within the images, the longer trends and more significant bar migration patterns are visible and correspond closely to the outer bar state transitions.

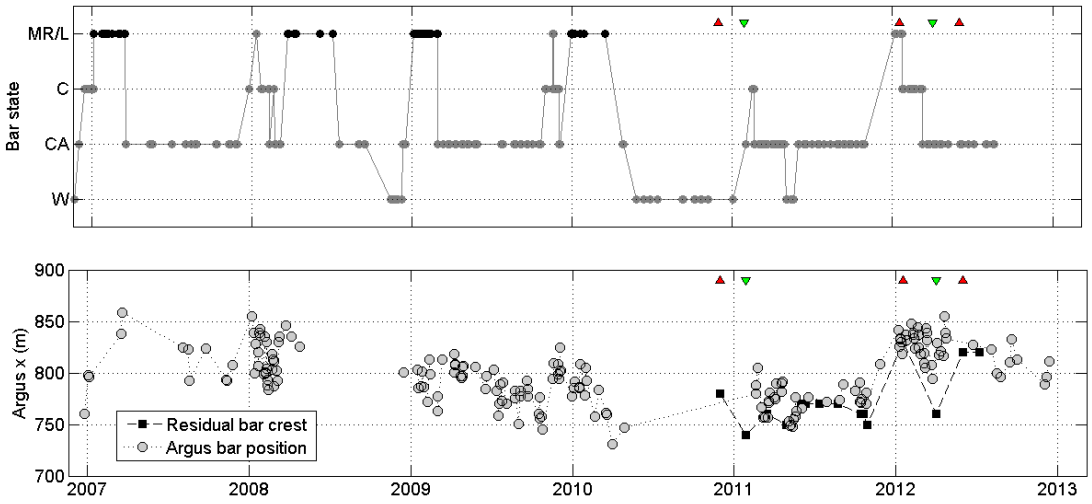

Figure **15** – *Top panel shows 6-year time series of outer bar type (cf. Figure **11**). The 5 outer sand bar types are MR = Mega Rip (black circles); L = Longshore (grey circles); C = Crescentic; CA = Crescentic Attached; and W = Welded. Lower panel shows corresponding time series of the cross-shore position of the outer bar derived from rectified Argus images (grey circles). The black squares in the lower panel represent the outer bar position derived from the bathymetric surveys (cf. Figure **8**). The red (upward pointing) and green (downward pointing) triangles in the bottom panel indicate significant offshore and onshore outer bar migration, respectively, observed from the bathymetric surveys.*

6. RELATING MORPHOLOGICAL RESPONSE TO HYDRODYNAMIC FORCING

6.1 Beach and nearshore morphology

A number of parameters were considered to identify the forcing for the observed outer bar morphological response. The time series of wave parameters were first averaged to provide daily means and then the following average parameters were computed for each inter-survey period: mean H_s; mean wave steepness H_s/L (where L is the wave length computed from the dispersion relationship using the mean wave period T_m); the deep water wave power P ($\propto H_s^2 T$ and computed using linear wave theory) from the dependency observed by Davidson et al. (2013); and the dimensionless fall velocity Ω (Gourlay, 1968), using a mean sediment fall velocity of w_s = 0.04 m s^{-1}. Figure **16** compares time series of the wave forcing parameters with the response of the outer bar. Although there appears to be a distinct anti-phase relationship between the forcing parameters and the outer bar response, none of the forcing parameters provide discrimination between all offshore and onshore bar migration events. The second offshore migration event during winter 2011/2012 can be correlated to energetic wave conditions (maximum H_s, H/L, P and Ω), but the first offshore migration event at the end of 2010 occurred under relatively mild wave conditions. It may be suggested that the change in wave conditions is more relevant in driving bar morphological change than the absolute values of the wave parameters: e.g., all offshore migration events occurred following an increase in H/L, whereas all onshore migration events coincided with falling H/L values.

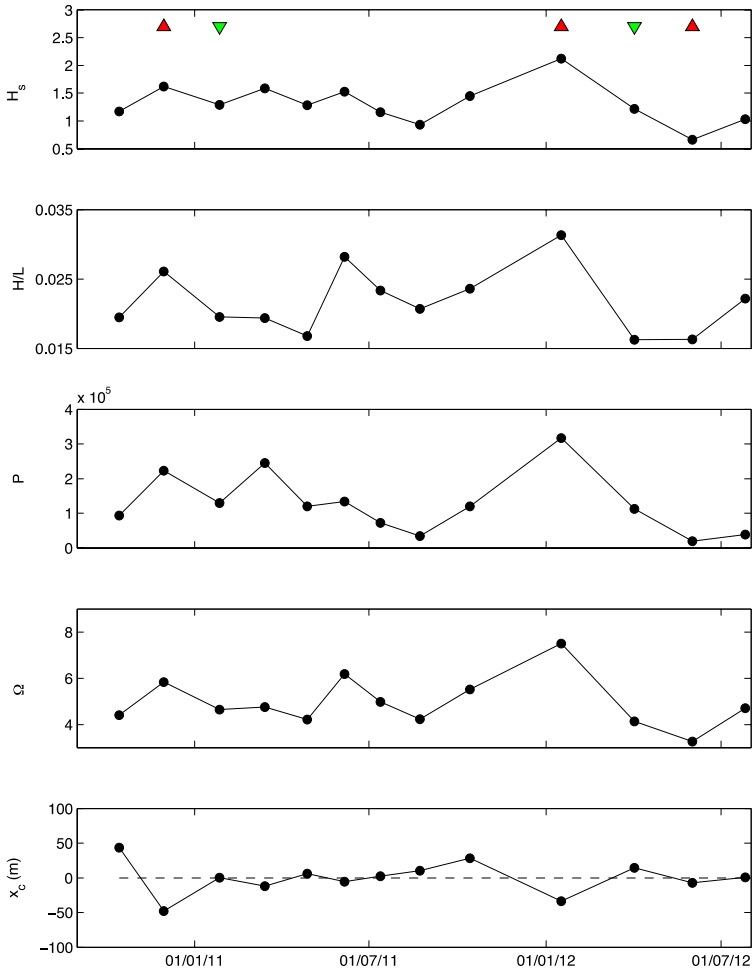

Figure **16** – *Integrated wave parameters based on daily-mean values for the inter-survey periods. From top to bottom: mean* H_s*, mean wave steepness* H/L*, mean wave power* P*, mean dimensionless fall velocity* Ω *and detrended observed bar migration. The red (upward pointing) and green (downward pointing) triangles in the top panel indicate significant offshore and onshore outer bar migration, respectively.*

If changes in the wave conditions are more relevant in driving bar behaviour than actual wave parameters, an equilibrium type of response model, involving deviations from antecedent wave conditions is worth pursuing (e.g., Yates et al., 2009; Davidson et al., 2013; Castelle et al., 2014). Following Davidson et al. (2013), bar dynamics are related to the product of the wave energy flux P and a disequilibrium term (Ω_m - Ω), where Ω_m is the background antecedent value for Ω, and Ω represents the instantaneous value. In recognition that large (small) values of Ω occur under energetic (calm) wave conditions, it can be posited that offshore outer bar migration occurs when wave conditions are more energetic that the antecedent conditions ($\Omega > \Omega_m$) and onshore outer bar migration is occurs when conditions are calmer than the antecedent conditions ($\Omega < \Omega_m$,). The instantaneous Ω was computed for a 30-day period immediately prior to each survey using the daily-mean Perranporth DWR data and four formulations for the background antecedent Ω_m were considered: (1) the long-term mean Ω over the length of the survey period; (2) the 120-day mean of the 4-month backward-time moving-average Ω immediately prior to each survey; (3) an optimised backward-time moving-average Ω immediately prior to each survey; and (4) a weighted-mean Ω computed following Davidson et al. (2013) with a relaxation time factor ϕ of 233 days and a window length $D = 2\phi$. A 4-month period was selected for (2) because it corresponds to the NAO-averaging period, to be discussed later. The optimum length of the backward-time moving average in (3) and the value of ϕ used in (4) were 270-days and 233-days, respectively; both were determined by optimising the model against the observed bar migration events. The disequilibrium forcing term $P^{0.5}(\Omega_m - \Omega)$ was computed for each survey and was compared to the detrended time series of the outer bar position (Figure **17**).

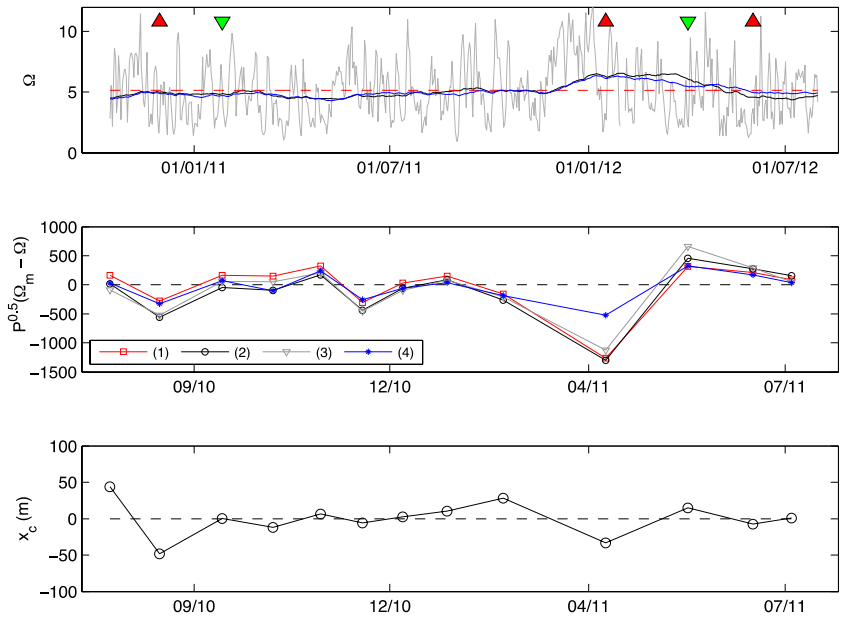

Figure **17** – *Top panel shows time series of instantaneous dimensionless fall velocity Ω (grey line), Ω_m 4-month backwards-time moving-average Ω (black line), mean annual Ω (horizontal red dashed line) and optimised weighted-mean Ω (blue line). Middle panel shows time series of disequilibrium parameter* $P^{0.5}(\Omega_m - \Omega)$ *computed using the mean annual Ω (red line with squares), deviation from the 4-month average Ω (black line with circles), optimised Ω (grey line with triangles) and optimised weighted-mean (blue line with asterisk). Bottom panel shows time series of de-trended outer bar position x_c. The red (upward pointing) and green (downward pointing) triangles in the bottom panel indicate significant offshore and onshore outer bar migration, respectively.*

The disequilibrium model performs remarkably well in predicting the change in bar position, with the two large offshore migration events associated with the strongly negative values of $P^{0.5}(\Omega_m - \Omega)$ and the significant onshore events linked to positive values of $P^{0.5}(\Omega_m - \Omega)$. The correlations between the disequilibrium parameter and the observed and detrended outer bar position using the annual-mean Ω_m, 4-month moving-average Ω_m, optimised moving-average Ω_m and weighted-mean Ω_m have r^2 = 0.29, 0.27, 0.33 and 0.31, respectively (p-values = 0.055, 0.07, 0.039 and 0.049). For comparison, if the monthly wave parameters in Figure **16** are regressed against the observed and detrended bar position, the r^2 values are 0.23, 0.15, 0.35 and 0.24 for H_s, H/L, P and Ω, respectively.

6.2 Outer bar migration and bar type transitions

Using a 2-year long time series of wave and morphological observations, it was demonstrated that bar position and dynamics can be explained to some degree by wave energy deviations from longer-term antecedent wave conditions parameterised through $P^{0.5}(\Omega_m - \Omega)$ (Figure **17**). The 53-year time series of WWIII modelled wave conditions and the winter North Atlantic Oscillation (NAO) index was used to show that above-average (below-average) winter wave conditions are significantly correlated to positive (negative) winter NAO indices (Figure **7**). Using a 6-year time series of measured wave data it was further illustrated that the winter wave climate in the region is strongly controlled by storms (Figure **6**). Finally, 15 years of Argus video data were used to generate a time series of outer bar types showing a common occurrence of annual cycles of upstate and downstate outer bar transitions (Figure **11**). These various strands of information are combined in Figure **18**, which relates the outer bar type observations to modelled and observed wave conditions, the occurrence of storms, the disequilibrium parameter and the winter NAO index.

Inspection of the top two panels of Figure **18** reveals that there is a strong, and unsurprising, correlation between storm frequency and intensity, and the winter wave height, and that there is also a strong correlation with the winter NAO index (e.g., most energetic winters 2006/2007 and 2011/2012; least energetic winters 2005/2006 and 2010/2011). The strong seasonal variation in the significant wave height H_s imposed by the winter storms is reflected in the time series of the disequilibrium parameter $P^{0.5}(\Omega_m - \Omega)$ plotted in the third panel of Figure **18**. The seasonal cycle in $P^{0.5}(\Omega_m - \Omega)$ is strongly asymmetrical, with significantly greater disequilibrium during the winter months ($P^{0.5}(\Omega_m - \Omega) < -400$), than during the summer months ($P^{0.5}(\Omega_m - \Omega) < 200$). The inter-annual variability in wave conditions and storminess is reflected in that of the $P^{0.5}(\Omega_m - \Omega)$ time series. The two most (2007/2008 and 2011/2012) and least (2005/2006 and

2010/2011) energetic winters referred to earlier are also characterised by the largest and smallest negative values of $P^{0.5}(\Omega_m - \Omega)$, respectively. The real challenge is whether the observed bar states and the bar state transitions can be related to the various wave forcings. The bottom panel of Figure **18** reveals that an upstate outer bar state transition (from W, CA or C to L or MR) occurred for 14 out of 16 winters. The only winters where the outer bar was not observed to reach the most erosional state (L or MR) was during 2005/2006 and 2010/2011, which are characterised by the lowest winter H_s values, negative NAO indices and the smallest negative values for the winter $P^{0.5}(\Omega_m - \Omega)$. There are cases where the outer bar reaches the most erosional state under significantly negative winter NAO (2001/2001 and 2009/2010), but, in both cases the initial upstate transition was initiated during the preceding high-energy autumn period. In the case of 2009/2010, the winter period was also preceded by the most energetic summer restricting accretion (downstate bar transition) and facilitating up-state transition over the energetic 2009 autumn period.

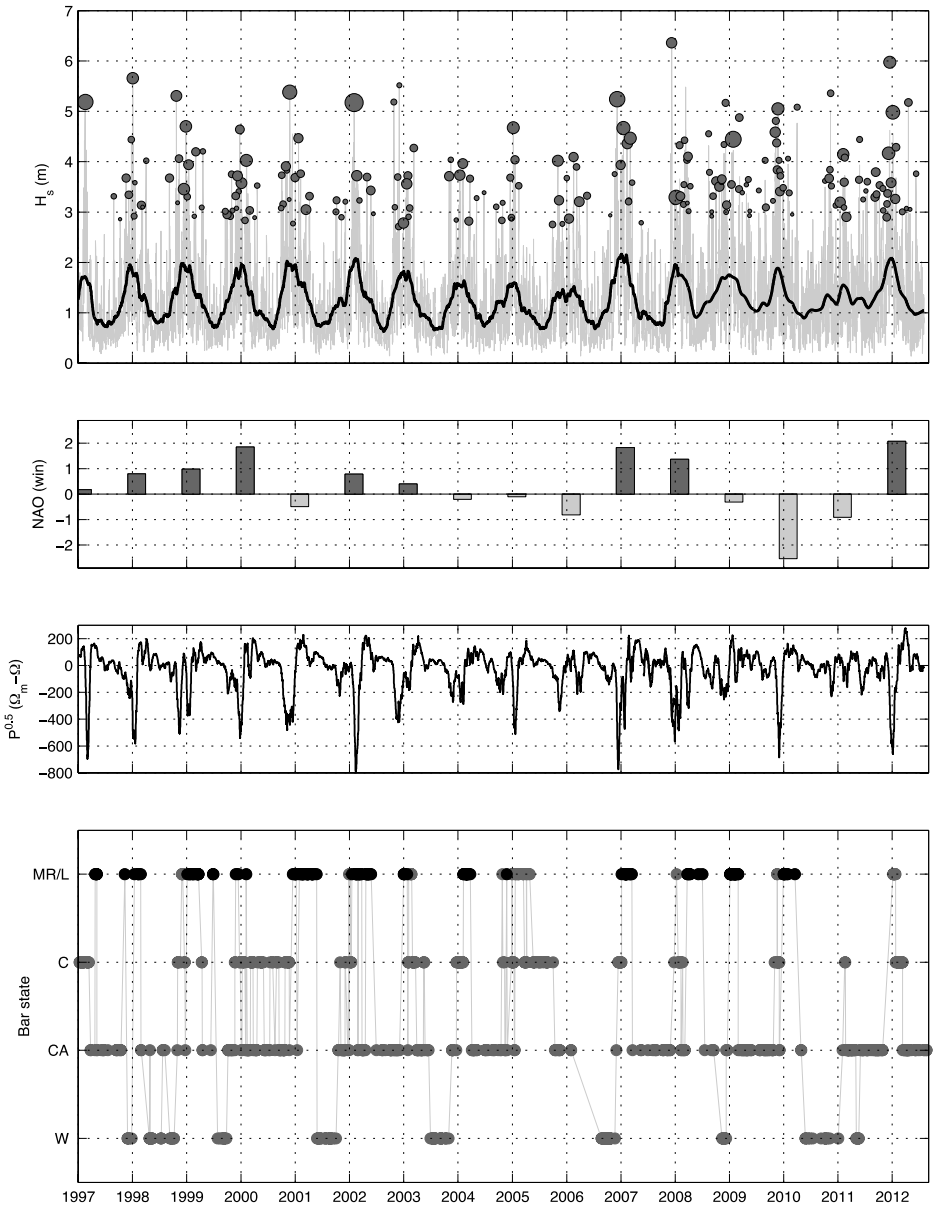

Figure **18** – *Top panel shows time series of 6-hourly* H_s *(grey line) and 4-month moving average of* H_s *(black line). The grey bubbles are storm events (*$H_s > H_{s,95\%}$*), whereby the size of the bubbles is proportional to storm duration based on* $H_{s,75\%}$ *cut-off either side of storm maximum. Data from 1997 to 2006 are WWIII modelled data, while data from 2007 to 2013 are wave data measured by the nearshore waverider buoy at Perranporth. Modelled wave heights have been adjusted so they are comparable with the measured wave heights. Second panel shows the 4-monthly averaged winter NAO index from Jones et al. (1997), extended by the Climatic Research Unit, University of East Anglia. Third panel shows the disequilibrium parameter* $P^{0.5}(\Omega_m - \Omega)$ *computed as the deviation of the 1-month average* Ω *from the 4-month antecedent average* Ω_m*. Bottom panel shows time series of outer bar type derived from Argus video images. The 5 outer sand bar types are MR = Mega Rip (black circles); L = Longshore (grey circles); C = Crescentic; CA = Crescentic Attached; and W = Welded. Upstate and downstate transitions represent moving up and down the diagram, respectively.*

7. DISCUSSION AND CONCLUSIONS

Perranporth is double-barred beach located on the north Cornish coast subjected to macrotidal conditions and an energetic shore-normally incident wave climate. The inner bar system is relatively subdued, three-dimensional and mostly characterised by transverse bar-rip morphology with rip currents active during low tide (Austin et al., 2010, 2014; Scott et al., 2014). The outer bar is more pronounced and most frequently assumes a crescentic bar shape with the horns attached to the low tide shoreline (Figure **8**). The inner and outer bar systems exhibit an out-of-phase relationship with the landward pointing horns of the outer bar coinciding with the seaward pointing salients associated with the inner bar system. A similar configuration was found by Price and Ruessink (2011) along the double-barred Gold Coast in Australia and is attributed to the dominance of parallel wave approach (Castelle et al., 2010a, b). Compared to other beaches described in the literature, Perranporth is most similar to Truc Vert (Castelle et al., 2007; Senechal et al., 2009; Coco et al., 2014), although the latter beach is characterised by more energetic wave conditions and a smaller tide range. There is no obvious effect of geological control on the beach morphology (cf., Jackson et al., 2005; Loureiro et al., 2012; van de Lageweg et al., 2013); however, the beach is quite long (c. 3.5 km; Figure **1**) and can be considered uninterrupted, despite being embayed.

Analysis of a morphological data set, comprising 2 years of inter- and subtidal morphological surveys and 16 years of Argus video data, indicates that the beach morphology is highly variable. Over the 2 year survey period, the subtidal zone and the region around the MLWS was significantly more dynamic (envelope of vertical change c. 2 m) than the intertidal region and the upper beach (envelope of vertical change < 1 m) (Figure **12**). By the end of the survey period, the subtidal region had gained 150,000–200,000 m^3 of sediment, while the intertidal region showed no significant difference between the start and end of the survey period (Figure **14**). This suggests that on beaches like Perranporth intertidal beach surveys will only provide partial insight into the beach dynamics and nearshore sediment budget (cf., Poate et al., 2014). Using the Argus video data, five bar states were identified for the outer bar (Figure **10**): welded bar (W), crescentic attached bar (CA), crescentic bar (C), longshore bar (L) and longshore bar dissected by mega rips (MR). Upstate transition of the outer bar (W → CA → C → L/MR), characterised by offshore migration and straightening of the outer bar, requires an extended period of energetic wave action (e.g., a sequence of storms); a downstate transition represents the opposite sequence and occurs following an extended period of calm wave conditions (cf., Poate et al., 2014; Figure **11**). Such upstate and downstate sequences have been reported previously for double-barred beaches in micro- and mesotidal settings (e.g., Castelle et al., 2007; Coco et al., 2014), but have not been identified previously for macrotidal beaches. On many sites characterised with multiple bar morphology, bar systems exhibit a bar-cycle, with time scale *O*(5–10 years), characterised by formation at the shoreline followed by intermittent offshore migration, and finally disappearance of the outer bar (e.g., Ruessink et al., 2003). There is no evidence that the bar systems on Perranporth exhibits such behaviour. Finally, there is some indication that the inner and outer bar morphology migrates alongshore towards the south at a rate of c. 600 m yr^{-1} (Figure **13**), but 2 years of data may not be representative of the alongshore bar behaviour.

Modal beach morphological state and morphological variability must be related to the hydrodynamic forcing. The effect of surge-related water-level variations is expected to be limited due to their restricted range (+/- 0.5 m; Figure **5.surge**) and, although the tidal regime is important for the modal beach state, it is unlikely that neap-to-spring tidal variation plays a significant role in beach dynamics. This leaves the wave climate as the key hydrodynamic factor in controlling beach morphological change. A comprehensive analysis of 7 years of inshore directional wave data reveals a seasonally variable wave climate characterised by an average winter and summer significant wave height H_s of 1.6 m and 1.1 m, respectively (Figure **6**). Defining a storm as an event where H_s exceeds the 0.95 quantile (2.83 m), a total of 107 storms were identified over the 7-year period, representing an average of 15 storms per year (Figure **6**). Storms mainly occur during the winter months and the average storm peak H_s and storm duration is 3.8 m and 66 hrs, respectively. In addition to the *intra-annual* (seasonal) variability, the winter wave conditions and storminess also exhibit a pronounced *inter-annual* variability with for some years a winter H_s > 2 m, while in other years the winter H_s barely exceeds 1.5 m (Figure **18**). By extending the observational wave time series with WWIII modelled wave data, it was found that the inter-annual wave variability is significantly correlated with the winter North Atlantic Oscillation (NAO) index (Figure **7**). The most (least) energetic winters are associated with positive (negative) NAO indices, and the winter NAO itself shows a weak 5-year cyclicity. Such linkage between winter wave conditions and winter NAO has previously been demonstrated by Dodet et al. (2010) and Woolf et al. (2002).

The dimensionless fall velocity Ω is a widely used parameter for classifying beaches in a range of environments (e.g., Scott et al., 2011). As a consequence of wave variability, Ω varies considerably over a year, ranging between 2 and 10, with a long-term average of 5 (Figure **17**). The overall intermediate morphodynamic state of the beach fits quite well

with previous models based on Ω (Wright and Short, 1984; Masselink and Short, 1993), but the configuration of the outer bar morphology changes over a much longer time scale (monthly-to-annual) than the daily-to-weekly variations in Ω. An extended period of energetic wave action appears to be required to bring about an upstate bar transition (W → CA → C → L/MR) and the bar then remains arrested for a significant amount of time, requiring several months of low wave conditions to induce a down state transition (L/MR → C → CA → W). It is suggested that this can be attributed to the larger tidal range at the study site. The outer bar morphology is only active for part of the tidal cycle (several hours around low tide), considerably extending relaxation times and slowing down morphological response (cf. Masselink, 1993).

The configuration and position of the outer bar are related: the more upstate (downstate) bar types are associated with a more offshore (onshore) bar position. A simple model, based on Davidson et al. (2013), was formulated to relate the outer bar position to a disequilibrium forcing term $P^{0.5}(\Omega_m - \Omega)$, where P is wave power, Ω_m is the background antecedent value for Ω (computed either as the long-term average or the 4-month average), and Ω represents the instantaneous value. Both Ω and P were computed for a 30-day period immediately prior to each survey. It was found that the disequilibrium term $P^{0.5}(\Omega_m - \Omega)$ was significantly related to the detrended outer bar position and that offshore outer bar migration occurs when wave conditions are more energetic that the antecedent conditions ($\Omega > \Omega_m$), while onshore outer bar migration is occurs when conditions are calmer than the antecedent conditions ($\Omega < \Omega_m$,) (Figure **17**). It is noteworthy that the optimised time windows for Ω_m of 233 and 270 days are very similar to the findings of Davidson et al. (2013) for the Gold Coast, suggesting morphodynamic parallels between the two sites, despite the large difference in tidal range. The model has considerable potential as a predictive tool, but a longer and higher resolution observational time series (at least monthly observations over a period > 5 years) is required to further develop and validate the model (cf. Castelle et al., 2014).

This investigation demonstrates that: (1) outer bar configuration and dynamics are related to wave forcing; and (2) inter-annual variability in winter wave condition and storminess are related to the winter North Atlantic Oscillation (NAO) index. Therefore, there is a correlation between long-term beach morphology and winter NAO. Typically, the outer bar undergoes an upstate transition over the winter months and a downstate transition over the summer months. The upstate end member (L or MR) was attained sometime during the winter months for 14 out of the 16 years of monitoring; the outer bar remained attached to the low tide shoreline over the winter 2005/2006 and 2010/2011. These two winters with incomplete upstate cycles were characterised by the lowest winter wave conditions and negative NAO indices (Figure **18**). This is the first time that NAO has been correlated with the actual beach state and nearshore bar configuration.

ACKNOWLEDGEMENTS

We would like to thank our excellent field and technical team for supporting the many and various field efforts on Perranporth over the past decade, especially our Senior Technical Officer Peter Ganderton. We would also like to thank the RNLI and the Perranporth YHA for their ongoing support for our research at Perranporth. This research was funded by the NERC–RNLI partnership grant NE/H004262/1, *Dynamics of Rip Currents and Implications for Beach Safety* (DRIBS).

REFERENCES

Aagaard, T., 1988. A study on nearshore bar dynamics in a low-energy environment: Northern Zealand, Denmark. *Journal of Coastal Research*, 4, 115-128.

Aagaard, T. and Kroon, A., 2007. Mesoscale behaviour of multiple bar systems: net onshore or net offshore migration. *Proceedings Coastal Sediments 2007*, ASCE, 2124-2136.

Armaroli, C. and Ciavola, P., 2011. Dynamics of a nearshore bar system in the northern Adriatic: A video-based morphological classification. *Geomorphology*, 126, 201-216.

Austin, M.J., Scott, T.M., Brown, J., Brown J., Masselink, G. and Russell, P.E., 2010. Temporal observations of rip current circulation on a macro-tidal beach. *Continental Shelf Research*, 30, 1149–1165.

Austin, M.J., Scott, T.M., Russell, P.E. and Masselink, G., 2013. Rip current prediction: development, validation, and evaluation of an operational tool. *Journal of Coastal Research*, 29, 283-300.

Austin, M.J., Masselink, G., Scott, T.M. and Russell, P.E., 2014. Water-level controls on macro-tidal rip currents. *Continental Shelf Research*, 75, 28–40.

Butt, T., Russell, P.E. and Turner, I., 2001. The influence of swash infiltration-exfiltration on beach face sediment transport: onshore or offshore? *Coastal Engineering*, 42, 35-52.

Butt, T., and Russell, P.E., 1999, Sediment transport mechanisms in high energy swash. *Marine Geology*, 161, 361-375.
Butt, T., Miles, J., Ganderton, P. and Russell, P.E., 2002, A simple method for calibrating optical backscatter sensors in high concentrations of non-cohesive sediments. *Marine Geology*, 192, 419-424.
Butt, T., Russell, P.E., Miles, J. and Turner, I.L., 2007. Sediment transport processes in the swash zone of sandy beaches. International Coastal Symposium. *Journal of Coastal Research*, SI 50, 636-640.
Butt, T. and Russell, P.E., 2005. Observations of hydraulic jumps in high energy swash. *Journal of Coastal Research*, 21, 1219-1227.
Butt, T, Russell, P.E., Puleo, J. and Masselink, G., 2005. The application of Bagnold-type sediment transport models in the swash zone. *Journal of Coastal Research*, 21, 887-895.
Castelle, B., Bonneton, P., Dupuis, H., & Sénéchal, N. (2007). Double bar beach dynamics on the high-energy meso-macrotidal French Aquitanian Coast: A review. *Marine Geology, 245*(1-4), 141–159.
Castelle, B., Ruessink, B.G., Bonneton, P., Marieu, V., Bruneau, N. and Price, T.D., 2010a. Coupling mechanisms in double sandbar systems. Part 1: patterns and physical explanation. Earth Surface Processes and Landforms, 35, 476-486.
Castelle, B., Ruessink, B.G., Bonneton, P., Marieu, V., Bruneau, N. and Price, T.D., 2010b. Coupling mechanisms in double sandbar systems. Part 2: impact on alongshore variability of inner-bar rip channels. *Earth Surface Processes and Landforms*, 35, 771-781.
Castelle, B., Marieu, V., Bujan, S., Ferreira, S., Parisot, J.-P., Capo, S., Sénéchal, N. and Chouzenoux, T., 2014. Equilibrium shoreline modelling of a high-energy meso-macrotidal multiple-barred beach. *Marine Geology*, 347, 85-94.
Coco, G., Senechal, N., Rejas, A., Bryan, K.R., Capo, S., Parisot, J.P., Brown, J.A. and MacMahan, J.H.M., 2014. Beach response to a sequence of storms. *Geomorphology*, 204, 493-501.
Davidson, M.A., Splinter, K.D. and Turner I.L., 2013. A simple equilibrium model for predicting shoreline change. *Coastal Engineering*, 73, 191-202.
Davidson, M., Huntley, D., Holman, R. and George, K., 1997. The evaluation of large-scale (km) intertidal beach morphology on a macrotidal beach using video images. *Proceedings Coastal Dynamics '97*, ASCE, 385-394.
Dean, R.G., 1973. Heuristic models of sand transport in the surf zone. *Proceedings of the Conference on Coastal Engineering Dynamics in the Surf Zone*, Instution of Engineers, 208– 214.
Dodet, G., Bertin, X. and Taborda, R., 2010. Wave climate variability in the North-East Atlantic Ocean over the last six decades. *Ocean Modelling*, 31, 120-131.
Gourlay, M.R., 1968. *Beach and Dune Erosion Tests*. Rep. M935/M936, Delft Hydraulics Laboratory, Delft, Netherlands.
Hegge, B. and Masselink, G., 1996. Spectral analysis of geomorphic time series: Auto-Spectrum. Earth Surface Processes and Landforms, 21, 1021-1040.
Holman, R.A. and Stanley, J., 2007. The history and technical capabilities of Argus. *Coastal Engineering*, 54, 477-491.
Holland, K.T., Holman, R.A., Lippmann, T.C., Stanley, J. and Plant, N., 1997. Practical use of video imagery in nearshore oceanographic field studies. *Oceanic Engineering*, 22, 81-92.
Hurrell, J.W., 1995. Decadal trends in the North Atlantic Oscillation: regional temperatures and precipitations. Science 269, 676–679.
Jackson, N.L., Nordstrom, K.F., Eliot, I.G. and Masselink, G., 2002. 'Low energy' sandy beaches in marine and estuarine environments: a review. *Geomorphology*, 48, 147-162.
Jackson, D., Cooper, A. and del Rio, L., 2005. Geological control of beach morphodynamic state. *Marine Geology*, 216, 297-314.
Jago, C.F. and Hardisty, J., 1984. Sedimentology and morphodynamics of a macrotidal beach, Pendine Sands, SW Wales. *Marine Geology*, 60, 123-154.
Thomas, T., Phillips, M.R., Williams, A.T. and Jenkins, R.E., 2012. Medium time-scale behaviour of adjacent embayed beaches: Influence of low energy external forcing. *Applied Geography*, 32, 265-280.
Jones, P.D., New, M., Parker, D.E., Martin, S. and Rigor, I.G., 1999. Surface air temperature and its changes over the past 150 years. *Reviews of Geophysics*, 37, 173-199.
Kingston, K.S., Ruessink, B.G., van Enckevort, I.M.J. and Davidson, M.A., 2000. Artificial neural network correction of remotely sensed sandbar location. *Marine Geology*, 169, 137-160.
Lanckriet, T., Puleo, J.A. and Waite, N., 2013. A conductivity concentration profiler for sheet flow sediment transport. *Oceanic Engineering*, 38, 55-70.
Lippmann, T.C. and Holman, R.A., 1990. The spatial and temporal varability of sand bar morphology. *Journal of Geophysical Research*, 95, 11575-11590.
Loureiro, C., Ferreira, Ó. and Cooper, J.A.G., 2012. Geologically constrained morphological variability and boundary effects on embayed beaches. *Marine Geology*, 329-331, 1-15.

Lygre, A., and Krogstad, H. E., 1986. , Maximum entropy estimation of the directional distribution in ocean wave spectra. *Journal of Physical Oceanography*, 16, 2052-2060.
Masselink, G. and Russell, P., 2006. Flow velocities, sediment transport and morphological change in the swash zone of two contrasting beaches. *Marine Geology*, 227, 227-240.
Masselink, G., Evans, D., Hughes, M.G. and Russell, P., 2005. Suspended sediment transport in the swash zone of a dissipative beach. *Marine Geology*, 216, 169-189.
Masselink, G. and Anthony, E.J., 2001. Location and height of intertidal bars on macrotidal ridge and runnel beaches. *Earth Surface Processes and Landforms*, 26, 759-774.
Masselink, G. and Hegge, B., 1995. Morphodynamics of meso- and macrotidal beaches: examples from central Queensland, Australia. *Marine Geology*, 129, 1-23.
Masselink, G. and Short, A.D., 1993. The effect of tide range on beach morphodynamics and morphology: A conceptual beach model. *Journal of Coastal Research*, 9, 785-800.
Masselink, G., 1993. Simulating the effects of tides on beach morphodynamics. *Journal of Coastal Research*, SI15, 180-197.
Osborn T.J., 2006. Recent variations in the winter North Atlantic Oscillation. *Weather* 61, 353-355.
Price, T.D. and Ruessink, B.G., 2011. State dynamics of a double sandbar system. *Continental Shelf Research*, 31, 659-674.
Plant, N.G., Holland, K.T. and Puleo, J.A., 2002. Analysis of the scale of errors in nearshore bathymetric data. *Marine Geology*, 191, 71-86.
Poate, T., Masselink, G., Russell, P., Austin, M., 2014. Morphodynamic variability of high-energy macrotidal beaches, Cornwall, UK, Marine Geology, 350, 97-111.
Puleo, J.A., Lanckriet, T. and Blenkinsopp, C., 2014. Bed level fluctuations in the inner surf and swash zone of a dissipative beach. *Marine Geology*, 349, 99-112.
Ranasinghe, R., Symonds, G., Black, K. and Holman, R., 2004. Morphodynamics of intermediate beaches: a video imaging and numerical modelling study. *Coastal Engineering*, 51, 629-655.
Ruessink, B.G., Wijnberg, K.M., Holman, R.A., Kuriyama, Y. and Enckevort, I.M.J. van, 2003. Intersite comparison of interannual nearshore bar behavior. *Journal of Geophysical Research*, 108, 3249.
Ruessink, B.G., Walstra, D.J.R. and Southgate, H.N., 2003. Calibration and verification of a parametric wave model on a barred beaches. *Coastal Engineering*, 48, 139-149.
Ruessink, B.G. and Kroon, A., 1994. The behaviour of a multiple bar system in the nearshore zone of Terschelling: 1965-1993. *Marine Geology*, 121, 187-197.
Scott, T., Masselink, G., Austin, M.J. Russell, P.E., 2014. Controls on macrotidal rip current circulation and hazard. *Geomorphology*, http://dx.doi.org/10.1016/j.geomorph.2014.02.005.
Scott, T., Masselink, G. and Russell, P.E., 2011. Morphodynamic characteristics and classification of beaches in England and Wales. *Marine Geology*, 286, 1-20.
Sedrati, M. and Anthony, E.J., 2007. Storm-generated morphological change and longshore sand transport in the intertidal zone of a multi-barred macrotidal beach. *Marine Geology*, 244, 209-229.
Sénéchal, N., Gouriou, T., Castelle, B., Parisot, J.P., Capo, S., Bujan, S. and Howa, H., 2009. Morphodynamic response of a meso- to macro-tidal intermediate beach based on a long-term data set. *Geomorphology*, 107, 263-274.
Short, A.D., 1979. Three dimensional beach-stage model. *Journal of Geology*, 87, 553-571.
Short, A.D., 1985. Rip current type, spacing and persistence, Narrabeen Beach, Australia. *Marine Geology*, 65, 47-71.
Short, A.D., 1991. Macro-meso tidal beach morphodynamics: an overview. *Journal of Coastal Research*, 7, 417-436.
Short, A.D., 1992. Beach systems of the central Netherlands coast: Processes, morphology and structural impacts in a storm driven multi-bar system. *Marine Geology*, 107, 103-137.
Short, A.D. and Aagaard, T., 1993. Single and multi-bar beach change models. *Journal of Coastal Research* , SI15, 141-157.
Thorpe, A., Miles, J., Masselink, G., Russell, P., Scott, T., Austin, M., 2013. Sediment transport in rip currents on a macrotidal beach. 12th International Coastal Symposium, Plymouth, England, *Journal of Coastal Research*, SI65, 1880-1885
Thorpe, A., Miles, J., Masselink, G., Russell, P.E., 2014. Bedform dynamics in a rip current. 13th International Coastal Symposium, Durban, South Africa, *Journal of Coastal Research*, SI##.
Tolman, H. L., 2009. User manual and system documentation of WAVEWATCH III version 3.14. NOAA/NWS/NCEP/MMAB Technical Note 276, 194 p.
Tucker, M.J., 1950. Surf beats: Sea waves of 1 to 5 minute period. *Proceedings Royal Society London A*, 202, 565-573.
Van de Lageweg, W.I., Bryan, K., Coco, G. and Ruessink, B.,G., 2013. Obervations of shoreline-sandbar coupling on an embayed beach. *Marine Geology*, 344, 101-114.

van Enckevort, I.M.J., Ruessink, B.G., Coco, G., Suzuki, K., Turner, I.L., Plant, N.G. and Holman, R.A., 2004. Observations of nearshore crescentic sandbars. *Journal of Geophysical Research*, 109, C06028.

van Enckevort, I.M.J. and Ruessink, B.G., 2003. Video observations of nearshore bar behaviour. Part 1: alongshore uniform variability. *Continental Shelf Research*, 23, 501-512.

van Enckevort, I.M.J. and Ruessink, B.G., 2003. Video observations of nearshore bar behaviour. Part 2: alongshore non-uniform variability. *Continental Shelf Research*, 23, 513-532.

Van Houwelingen, S.T., Masselink, G. and Bullard, J.E., 2006. Characteristics and dynamics of multiple intertidal bars, north Lincolnshire, England. *Earth Surface Processes and Landforms*, 31, 428-443.

Van Houwelingen, S.T., Masselink, G. and Bullard, J.E., 2008. Dynamics of multiple intertidal bars over semi-diurnal and lunar tidal cycles, North Lincolnshire, England. *Earth Surface Processes and Landforms*, 33, 1473-1490.

Walstra, D.J.R., Reneirs, A.J.H.M., Ranasinghe, R., Roelvink, J.A. and Ruessink, B.G., 2012. On bar growth and decay during interannual net offshore migration. *Coastal Engineering*, 60, 190-200.

Woolf, D.K., P.G. Challenor and P.D. Cotton. (2002). The variability and predictability of North Atlantic wave climate. *Journal of Geophysical Research*, 107(C10), 3145,

Wright, L.D. and Short, A.D., 1984. Morphodynamic variability of surf zones and beaches: A synthesis. *Marine Geology*, 56, 93-118.

Wright, L.D., Short, A.D. and Green, M.O., 1985. Short-term changes in the morphodynamic states of beaches and surf zones: An empirical predictive model. *Marine Geology*, 62, 339-364.

Wright, L.D., Guza, R.T. and Short, A.D., 1982. Dynamics of a high-energy dissipative surf zone. *Marine Geology*, 45, 41-62.

Yates, M.L., Guza, R.T. and O'Reilly, W.C., 2009. Equilibrium shoreline response: observations and modelling. *Journal of Geophysical Research*, 114, CO9014.